


Standard and inverse site percolation of triangular tiles on triangular lattices: Isotropic and perfectly oriented deposition and removal

N. M. De La Cruz Feliz ^{1,2}, F. M. L. Pimentel ¹, N. De La Cruz Félix ^{1,2}, and A. J. Ramirez-Pastor ^{2,*}

¹*Instituto de Física (IFIS), Facultad de Ciencias, Universidad Autónoma de Santo Domingo-FONDOCYT, Av. Alma Mater, Santo Domingo 10105, Dominican Republic*

²*Departamento de Física, Instituto de Física Aplicada (INFAP), Universidad Nacional de San Luis - CONICET, Ejército de Los Andes 950, D5700HHW, San Luis, Argentina*



(Received 7 December 2023; accepted 13 February 2024; published 5 March 2024)

Numerical simulations and finite-size scaling analysis have been carried out to study standard and inverse percolation of triangular tiles of side k (k -tiles) on triangular lattices. In the case of standard percolation, the lattice is initially empty. Then, k -tiles are randomly and sequentially deposited on the lattice. In the case of inverse percolation, the process starts with an initial configuration where all lattice sites are occupied by single monomers (each monomer occupies one lattice site) and, consequently, the opposite sides of the lattice are connected by nearest-neighbor occupied sites. Then, the system is diluted by randomly removing k -tiles [composed by $k(k+1)/2$ monomers] from the lattice. Two schemes are used for the depositing and removing process: the isotropic scheme, where the deposition (removal) of the objects occurs with the same probability in any lattice direction; and the anisotropic (perfectly oriented or nematic) scheme, where one lattice direction is privileged for depositing (removing) the tiles. The study is conducted by following the behavior of four critical concentrations with the size k : (i) [(ii)] standard isotropic (oriented) percolation threshold $\theta_{c,k}$ ($\vartheta_{c,k}$), which represents the minimum concentration of occupied sites at which an infinite cluster of occupied nearest-neighbor sites extends from one side of the system to the other. $\theta_{c,k}$ ($\vartheta_{c,k}$) is reached by isotropic (oriented) deposition of k -tiles on an initially empty lattice; and (iii) [(iv)] inverse isotropic (oriented) percolation threshold $\theta_{c,k}^i$ ($\vartheta_{c,k}^i$), which corresponds to the maximum concentration of occupied sites for which connectivity disappears. $\theta_{c,k}^i$ ($\vartheta_{c,k}^i$) is reached after removing isotropic (completely aligned) k -tiles from an initially fully occupied lattice. The obtained results indicate that (1) $\theta_{c,k}$ ($\theta_{c,k}^i$) is an increasing (decreasing) function of k in the range $1 \leq k \leq 6$. For $k \geq 7$, all jammed configurations are nonpercolating (percolating) states and, consequently, the percolation phase transition disappears. (2) $\vartheta_{c,k}$ ($\vartheta_{c,k}^i$) show a behavior qualitatively similar to that observed for isotropic deposition. In this case, the minimum value of k at which the phase transition disappears is $k = 5$. (3) For both isotropic and perfectly oriented models, the curves of standard and inverse percolation thresholds are symmetric to each other with respect to the line $\theta(\vartheta) = 0.5$. Thus, a complementary property is found $\theta_{c,k} + \theta_{c,k}^i = 1$ (and $\vartheta_{c,k} + \vartheta_{c,k}^i = 1$), which has not been observed in other regular lattices. (4) Finally, in all cases, the jamming exponent ν_j was measured, being $\nu_j = 1$ regardless of the orientation (isotropic or nematic) or the size k considered. In addition, the accurate determination of the critical exponents ν , β , and γ reveals that the percolation phase transition involved in the system, which occurs for k varying between one and five (three) for isotropic (nematic) deposition scheme, has the same universality class as the standard percolation problem.

DOI: [10.1103/PhysRevE.109.034107](https://doi.org/10.1103/PhysRevE.109.034107)

I. INTRODUCTION

Studying the percolation phase transition occurring in random sequential adsorption (RSA) models of extended objects has been attracting a great deal of interest for a long time [1–6] because of its enormous number of applications in physics, chemistry, biology, and materials science, where connectivity and clustering play an important role [1,2,7–18]. Percolation theory is also known to provide a useful model for the analysis of more complicated models exhibiting phase transitions and critical phenomena [1–4].

In this type of studies, the objects are randomly and irreversibly deposited forming a single monolayer. The final state generated is a disordered state (known as jamming state), in which no more objects can be deposited due to the absence of free space of appropriate size and shape [5]. At intermediate densities, and under certain conditions, a transition occurs in the connectivity of the system [1]. Namely, for a precise value of the surface coverage, a cluster of nearest-neighbor sites extends from one side to the opposite side of the system. This particular value of concentration rate is named percolation threshold and it will be designated by the symbol θ_c ; at this critical concentration a second-order phase transition occurs, which is characterized by well-defined critical exponents [1]. Thus, a competition between percolation and jamming is established.

*antorami@unsl.edu.ar

Despite the simplicity of its definition, it is well known that it is a quite difficult matter to analytically determine the value of the jamming coverage and percolation threshold in the case of lattice models of extended objects deposited on two-dimensional (2D) lattices. The inherent complexity of the system still represents a major difficulty to the development of accurate analytical solutions, so computer simulations appear as a very important tool for studying this subject. In this direction, several authors investigated the isotropic deposition of straight rigid k -mers on 2D triangular lattices [19–26].

In Ref. [19], straight rigid k -mers were randomly and isotropically deposited on $L \times L$ triangular lattices. By computer simulations, the authors investigated the kinetics of the RSA for values of k in the interval $k = 1, \dots, 11$ and lattice size $L = 128$. The obtained results showed that the jamming coverage decreases monotonically as the k -mer size increases. Later, Budinski-Petković *et al.* [20] extended the study of linear k -mers on triangular lattices to larger lattices (lattices with linear size up to $L = 1000$), and objects of different sizes and shapes (linear segments; angled objects; triangles and hexagons). In the case of linear segments with values of k up to 20, and as reported in Ref. [19], the jamming coverage decreases monotonically approaching the asymptotic value of 0.56(1) for large values of k .

The percolation properties were also studied in Ref. [20], revealing that the percolation threshold decreases for shorter k -mers, reaches a value $\theta_c \approx 0.40$ for $k = 12$, and, it seems that θ_c does not significantly depend on k for larger k -mers; and (3) consequently, the ratio θ_c/θ_j increases with k . The effects of anisotropy [21] and the presence of defects [22] on the jamming behavior were also studied by the group of Budinski-Petković *et al.*

In the line of Refs. [19–22], four previous articles from our group [23–26] were devoted to the study jamming and percolation of straight rigid k -mers on triangular lattices. These papers will be referred to as Papers I, II, III, and IV, respectively. In Paper I, the work of Budinski-Petković *et al.* [19,20] was extended to larger lattices and longer objects: $L/k = 100, 150, 200, 300$ and $2 \leq k \leq 128$ for jamming calculations, and $L/k = 32, 40, 50, 75, 100$ and $2 \leq k \leq 256$ for percolation analysis. A more precise determination of the jamming coverage for large values of k was obtained, being this asymptotic limit 0.5976(5). On the other hand, a nonmonotonic size dependence was found for the percolation threshold, in accordance with previous data for square lattices [27–30]. In addition, the complete analysis of critical exponents performed in Paper I revealed that the percolation phase transition involved in the system has the same universality class of the ordinary random percolation, regardless of the value of k considered.

In Paper II, the problem of inverse percolation by removing straight rigid k -mers from 2D triangular lattices was investigated by using numerical simulations and finite-size scaling analysis. The study of the inverse percolation problem starts with all lattice sites occupied by single monomers (each monomer occupies one lattice site). Consequently, there always exists a spanning path through a sequence of nearest-neighbor occupied sites in the initial configuration. Then the system is diluted by randomly removing objects from the surface. The main objective is to obtain the maximum

concentration of occupied sites (minimum concentration of empty sites) at which the connectivity disappears. This value of the concentration is named the inverse percolation threshold θ_c^i . The term inverse is used simply to indicate that the size of the connected phase diminishes during the removing process and the percolation transition occurs between a percolating and a nonpercolating state.

The results in Paper II showed that (i) the inverse percolation threshold exhibits a nonmonotonic behavior as a function of the k -mer size: it grows from $k = 1$ to $k = 10$, presents a maximum at $k = 11$, and finally decreases and asymptotically converges towards a finite value for large segments. (ii) The percolating and nonpercolating phases extend to infinity in the space of the parameter k and, consequently, the model presents percolation transition in all the ranges of k . (iii) Finally, the phase transition occurring in the system belongs to the standard random percolation universality class regardless of the value of k considered.

More recently, in Paper III, the percolation behavior of aligned rigid rods of length k on 2D triangular lattices was investigated using numerical simulations. The linear k -mers were irreversibly deposited along one of the directions of the lattice. Interestingly, it was found that the percolation threshold displays an increasing trend when plotted against the k -mer size, for k ranging from 2 to 80. This result is strikingly different from the percolation behavior observed in square lattices, where the critical threshold decreases with k [31]. The exhaustive study of critical exponents confirmed that the phase transition in the system belongs to the standard random percolation universality class.

In Paper IV, the problem of standard and inverse percolation of straight rigid rods on triangular lattices was revisited using numerical simulations and finite-size scaling analysis. Two schemes were employed for the deposition and removal process: an isotropic and an anisotropic scheme. The former denotes a scheme where the deposition and removal of the linear objects occurs with the same probability in any lattice direction, whereas the latter corresponds to a scheme where one lattice direction is privileged for depositing (removing) the particles. The study was conducted by following the behavior of four critical concentrations with the size k : (i) [(ii)] standard isotropic (oriented) percolation threshold $\theta_{c,k}$ ($\vartheta_{c,k}$), which represents the minimum concentration of occupied sites at which an infinite cluster of occupied nearest-neighbor sites extends from one side of the system to the other. $\theta_{c,k}$ ($\vartheta_{c,k}$) is reached by isotropic (oriented) deposition of straight rigid k -mers on an initially empty lattice; and (iii) [(iv)] inverse isotropic (oriented) percolation threshold $\theta_{c,k}^i$ ($\vartheta_{c,k}^i$), which corresponds to the maximum concentration of occupied sites for which connectivity disappears. $\theta_{c,k}^i$ ($\vartheta_{c,k}^i$) is reached after removing isotropic (completely aligned) straight rigid k -mers from an initially fully occupied lattice. These four critical concentrations were determined for a wide range of k ($2 \leq k \leq 512$).

The results obtained in Paper IV revealed that (1) $\theta_{c,k}$ and $\theta_{c,k}^i$ exhibit a nonmonotonic dependence on k . Both decrease or increase respectively for small particle sizes, go through a minimum or maximum around $k = 11$ and finally asymptotically converge towards definite values for large segments: $\theta_{c,k \rightarrow \infty} = 0.500(2)$ and $\theta_{c,k \rightarrow \infty}^i = 0.500(1)$. This behavior

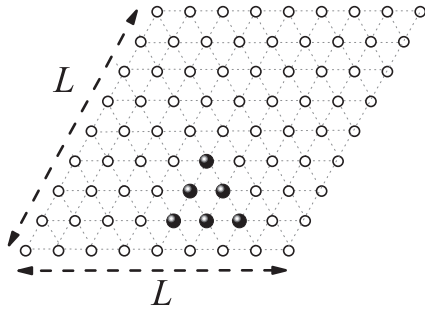


FIG. 1. Rhombus-shaped triangular lattice with $L = 9$. Open circles correspond to empty sites and solid spheres represent units belonging to a deposited 3-tile ($k = 3$).

occurs not only for straight rigid rods on triangular lattices but also for straight rigid rods on square lattices [27–30], as well as for the case of thermalized isotropic dispersions, where a maximum in the percolation threshold as a function of aspect ratio has been found [32]. (2) $\vartheta_{c,k}$ and $\vartheta_{c,k}^i$ display a monotonic behavior in terms of k . Both rapidly increase or decrease, respectively, for small particle sizes and asymptotically converge towards definite values for infinitely long k -mers: $\vartheta_{c,k \rightarrow \infty} = 0.5334(6)$ and $\vartheta_{c,k \rightarrow \infty}^i = 0.4666(6)$. (3) For both isotropic and perfectly oriented models, the curves of standard and inverse percolation thresholds are symmetric with respect to the line $\theta(\vartheta) = 0.5$. This symmetry implies a property of complementarity: $\theta_{c,k} + \theta_{c,k}^i = 1$ (and $\vartheta_{c,k} + \vartheta_{c,k}^i = 1$), which has not been observed in other regular lattices. This condition was verified analytically by using the exact enumeration of configurations for small systems. (4) Finally, in all cases, the critical concentration curves divide the θ space in a percolating region and a nonpercolating region. These phases extend to infinity in the space of the parameter k so that the model presents percolation transition for the whole range of k .

The aim of the present work is to extend previous studies to more compact objects such as triangular tiles of side k [objects occupying $k(k+1)/2$ sites on a triangular lattice, see Fig. 1]. In the case of square geometry, several studies have been carried out regarding jamming and percolation for square tiles of side k (objects occupying k^2 sites on a square lattice) which will serve as guide and comparison for our work [33–40]. In the cited articles, it was shown that (i) for systems consisting of $k \times k$ tiles with $k = 2$ and $k = 3$, clusters of particles in contact occur that span the whole lattice and percolate in the limit of an infinite system. For particles of linear size $k = 4$ and larger, it was found that only finite clusters exist, and, consequently, the percolation phase transition disappears [33–35]. (ii) The jamming concentration monotonically decreases and tends to $0.562\dots$ as the length of the squares increases [35–39]. (iii) The inverse percolation threshold is a decreasing function of k in the range ($1 \leq k \leq 4$). For $k \geq 5$, all jammed configurations are percolating states (the lattice remains connected even when the highest allowed concentration of removed sites is reached) [40]. (iv) Finally, standard and inverse percolation problems belong to the 2D random percolation universality class [35,40].

In the case of triangular tiles of side k (or k -tiles) deposited on triangular lattices (which is the subject of this paper), the

model allows us to incorporate the orientation of the deposited object as a new degree of freedom providing new properties. Despite this wide range of possibilities, the study of the jamming and percolation properties of k -tiles on triangular lattices has been restricted to isotropic deposition only. In this direction, in Ref. [20], the results for the percolation thresholds, jamming concentrations and their ratios were also given for the deposition of compact objects on a triangular lattice. It was found that while the percolation threshold monotonically decreases for elongated shapes, it monotonically increases with the object size for more compact shapes. For the particular case of triangular tiles of side k , the study in Ref. [20] showed that the percolation threshold is an increasing function of k in the range $1 \leq k \leq 5$. The problem of k -tiles on triangular lattices was recently addressed in the framework of the particle shape-controlled seeded growth model [41]. In Ref. [41], the authors considered needle-like objects and “wrapping” objects whose size is gradually increased by wrapping the walks in several different ways, making triangles, rhombuses, and hexagons. The results obtained for triangles (k -tiles) were consistent with those previously reported in Ref. [20].

In this work the problem of standard percolation of k -tiles isotropically deposited on 2D triangular lattices is revisited. The most important simulation results obtained in previous papers are used as a starting point. Then, the calculations are extended to three related models that have not been studied yet: (1) standard percolation of aligned k -tiles on a triangular lattice; (2) inverse percolation of isotropically removed triangles from a triangular lattice; and (3) inverse percolation of aligned k -tiles removed from triangular lattices. The new calculations represent not only quantitative expansion but also a qualitative advance in the description of the percolation properties of compact objects deposited on (removed from) triangular lattices.

The results and conclusions obtained here are backed by several features. First, the results obtained in Refs. [20,41] (standard percolation of k -tiles isotropically deposited on triangular lattices) were corroborated and extended to the critical exponents characterizing the universality of both the percolation transition (when possible) and the jamming transition.¹ Second, the functionality (in terms of k) of the inverse percolation threshold for k -tiles isotropically removed from triangular lattices is established here. The new data show that, in both standard and inverse problems, the percolation phase transition disappears for $k \geq 7$. Third, the present study shows that, in the isotropic case, the sum of standard and inverse percolation thresholds is equal to one for all value of k where the percolation phase transition exists ($1 \leq k \leq 6$). This complementarity property has not been observed so far in other regular lattices. Fourth, in the case of aligned k -tiles, the results of standard and inverse percolation thresholds versus k are presented. As in the isotropic case, there exists a value of $k = k_{\max}$ such that, for $k > k_{\max}$, the percolation phase transition disappears. $k_{\max} = 4$ for aligned k -tiles deposited

¹Even though it may be theoretically expected that the percolation transition in a system of k -tiles on triangular lattices belongs to the random percolation universality class, accurate numerical verification of this has not been done so far.

on (removed from) triangular lattices. These findings confirm the arguments presented in Ref. [42] about the interplay between jamming and percolation when the dimension of the depositing object is equal to the dimension of the substrate. In addition, the sum of standard and inverse percolation thresholds equals 1, confirming the generality of this behavior in triangular lattices.

The rest of the paper is organized as follows: In Sec. II, the standard problem of jamming and percolation of k -tiles on 2D triangular lattices is revisited. Calculations are extended to longer objects. In addition, new results are given for the inverse process of isotropically removing k -tiles from an initially fully occupied triangular lattice. The problem of standard and inverse percolation of aligned k -tiles is addressed in Sec. III. The analysis of the critical exponents and universality class is presented in Sec. IV. Finally, the conclusions are drawn in Sec. V.

II. STANDARD AND INVERSE PERCOLATION OF k TILES ON TRIANGULAR LATTICES: ISOTROPIC DEPOSITION (REMOVAL)

In this section we revisit the percolation problem of rigid triangular tiles isotropically deposited on triangular lattices, this time including the inverse percolation case and focusing on the complementarity property of the standard and inverse percolation thresholds: $\theta_c + \theta_c^i = 1$. For this purpose, new numerical simulations are presented in Sec. II C.

A. Model and basic definitions

The percolation problem is defined on a 2D triangular lattice. In the computer simulations, a rhombus-shaped system of $M = L \times L$ sites (L rows and L columns) is used (see Fig. 1). Each site can be empty (hole) or occupied. Occupied and empty sites are distributed with a concentration θ and θ^* ($= 1 - \theta$), respectively. Nearest-neighbor occupied sites form structures called clusters, and the distribution of these sites determines the probability of the existence of a large cluster (also called “infinite” cluster, inspired by the thermodynamic limit) that connects from one side of the lattice to the other.

Two procedures have been considered. In the first one, triangular tiles of side k (with $k \geq 2$) are deposited randomly, sequentially, and irreversibly on an initially empty lattice. This scheme, known as random sequential adsorption (RSA) [5], is as follows: (i) a starting site and one of the two (s_1, s_2) possible triangular structures (see Fig. 2) are randomly chosen. (ii) If, beginning at the chosen site, the $k(k + 1)/2$ sites belonging to the structure selected in (i) are empty, then a k -tile is deposited on those sites [the $k(k + 1)/2$ sites are marked as occupied]. Otherwise, the attempt is rejected. When N tiles are deposited, the concentration of occupied and empty sites is $\theta = k(k + 1)N/(2M)$ and $\theta^* = [M - k(k + 1)N/2]/M$, respectively.

In the second procedure, the process starts with a fully occupied lattice ($\theta = 1$ and $\theta^* = 0$). In the full occupation state, all lattice sites are occupied by single monomers (each monomer occupies one lattice site). Then, the system is diluted by randomly removing triangular objects from the lattice. The mechanism of dilution is as follows: (i) a set

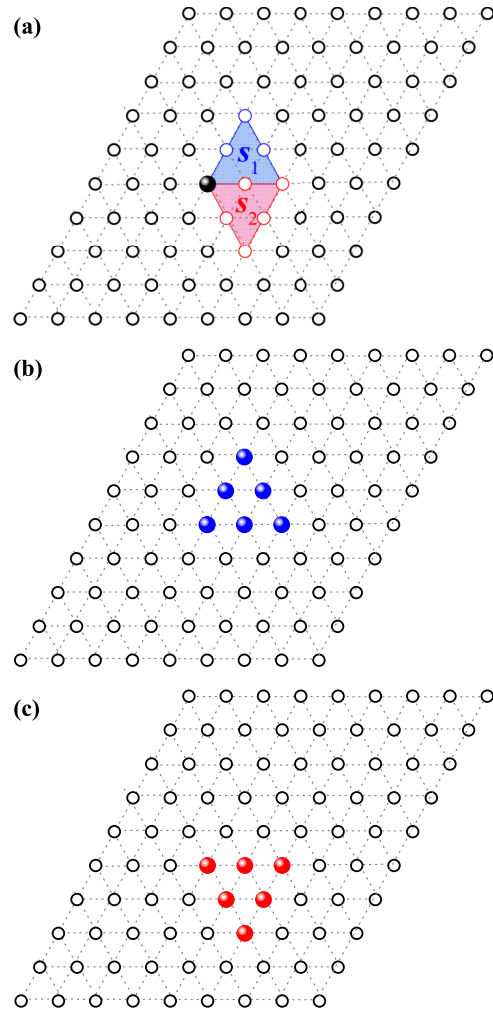


FIG. 2. Snapshots showing the elementary steps necessary to deposit a new k -tile on the lattice ($k = 3$ in the case of the figure). Panel (a) shows the starting site (solid sphere) and the two possible triangular structures s_1 (colored in blue tone) and s_2 (colored in red tone), according to the discussion in the text. If s_1 is selected, an up k -tile is deposited on the lattice [see panel (b)]. If s_2 is selected, a down k -tile is deposited on the lattice [see panel (c)].

of $k(k + 1)/2$ sites forming a k -tile is chosen at random; (ii) if the $k(k + 1)/2$ sites selected in step (i) are occupied by $k(k + 1)/2$ monomers, then those monomers are removed from the lattice. Otherwise, the attempt is rejected. When N tiles are removed, the concentration of particles holes is $\theta = [M - k(k + 1)N/2]/M$ and $\theta^* = kN(k + 1)/(2M)$.

In both the first process (deposition) and the second process (removal), periodic boundary conditions are considered. By using the first procedure (standard RSA), the lattice coverage is increased until finding a concentration at which a cluster of nearest-neighbor sites extends from one side to the opposite side of the system. This constitutes the so-called standard percolation problem, and the critical concentration rate is named standard percolation threshold.

On the other hand, when the k -tiles are removed from an initially fully occupied lattice (second procedure), the fraction of occupied sites decreases until reaching a concentration at which the connectivity disappears. The model of such a

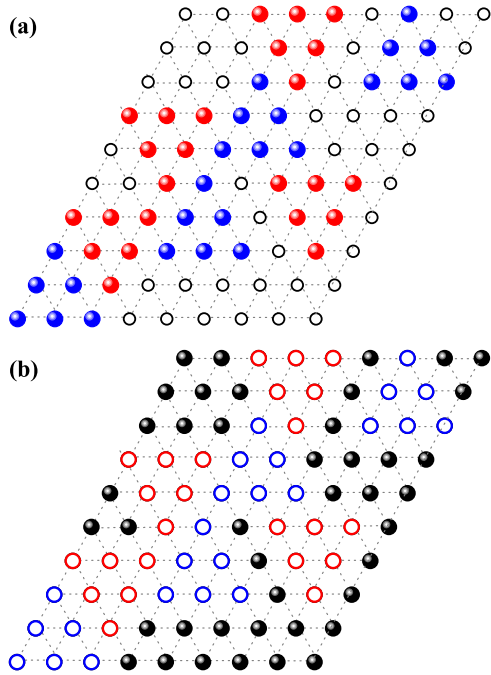


FIG. 3. (a) Schematic representation of a typical configuration obtained by isotropically depositing 3-tiles ($k = 3$) on a portion of a triangular lattice. Solid spheres represent the units (monomers) belonging to the deposited 3-tiles, and open circles correspond to empty sites. Up (down) triangles are denoted by blue (red). (b) Schematic representation of a typical configuration obtained by removing 3-tiles from an initially fully occupied portion of lattice. Solid spheres represent occupied sites (monomers), and open blue (red) circles indicate empty sites resulting from the removal of up (down) 3-tiles.

process can be thought of as an inverse percolation problem. The corresponding critical concentration is then named inverse percolation threshold. The term inverse is simply used to indicate that the size of the conductive phase diminishes during the removing process and the percolation transition occurs between a percolating and a nonpercolating state.

Typical configurations obtained from deposition and removal procedures are shown in Figs. 3(a) and 3(b). A system with $k = 3$ is depicted in the figure. In Fig. 3(a), solid spheres represent the units (monomers) belonging to the deposited 3-tiles and open circles correspond to empty sites. Up (down) triangles are denoted by blue (red). In Fig. 3(b), solid spheres represent occupied sites and open blue (red) circles indicate empty sites resulting from the removal of up (down) 3-tiles.

B. Jamming properties

Due to the increasing probability of blocking on the lattice by the already randomly deposited objects, the limiting or jamming coverage, $\theta_j \equiv \theta(t = \infty)$ is less than that corresponding one for close packing ($\theta_j < 1$). Note that $\theta(t)$ represents the dynamical fraction of lattice sites covered at time t by the deposited objects. Consequently, θ ranges from zero to θ_j for objects occupying more than one site, and the interplay between jamming and percolation must be considered.

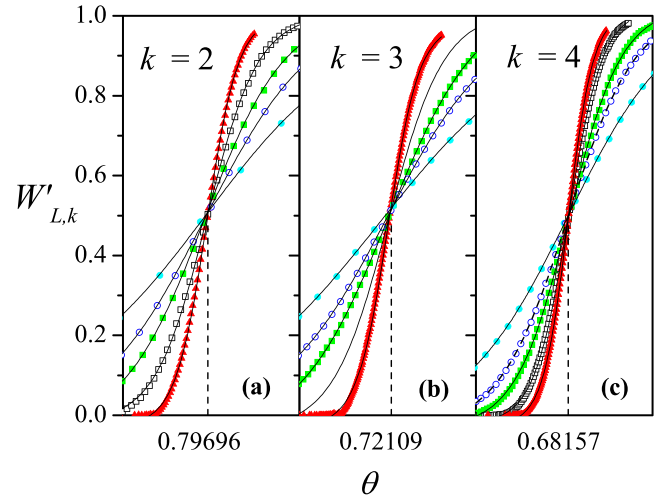


FIG. 4. Curves of the jamming probability $W'_{L,k}$ as a function of the fraction of occupied sites θ for three values of tile size, $k = 2, 3$, and 4 . Symbols represent simulation results and solid lines correspond to fitting curves using the error function. The lattice sizes are $L = 128$ (solid circles), 192 (open circles), 256 (solid squares), 384 (open squares), and 640 (solid triangles).

For the purpose of obtaining the jamming thresholds in terms of the size k , the probability $W_{L,k}(\theta)$ that a $L \times L$ lattice reaches a coverage θ has been calculated taking into account the numerical method introduced in Ref. [43]. It consists of the following steps: (a) the construction of the $L \times L$ lattices (initially empty) and (b) the deposition of k -tiles on each lattice up to the jamming limit $\theta_{j,k}$.

n runs of such two steps were carried out for each lattice size L . Then, the probability has been calculated as $W_{L,k}(\theta) = n_L(\theta)/n$, where $n_L(\theta)$ is the number of samples that reach a coverage θ . A set of $n = 2 \times 10^4$ independent samples were numerically prepared for different values of k and L : $k = 2-8$, $L = 128-640$; and $k = 12-32$, $L = 256-1280$. All of this requires extensive computer calculations which is one of the reasons that our results present better accuracy than previous reports.

As it will be shown in Sec. IV, it is useful to define the quantity $W'_{L,k} = 1 - W_{L,k}$, which can be fitted by the error function. In Fig. 4, the probability curves $W'_{L,k}(\theta)$ for different L values are shown for the cases $k = 2, 3$, and 4 . Symbols represent simulation results and solid lines correspond to fitting curves using the error function. Independent of the size k , the probability function $W'_{L,k}(\theta)$ renders a well-continued curve varying between zero for an empty lattice to 1 at the jamming condition. For finite systems the transition is never a step function so we have to observe it by the crossing of the $W'_{L,k}(\theta)$ functions assuming that the cases for $L \rightarrow \infty$ will also cross at that point. Then, based on the jamming probability functions for various L (see Fig. 4), we look for the interval where the curves cross each other. The center of this interval represents the jamming threshold ($\theta_{j,k}$) and the width of the interval is the error in the determination of $\theta_{j,k}$. In the figure, this interval is $(0.79694, 0.79698)$ for the case $k = 2$, $(0.72107, 0.72111)$ for the case $k = 3$ and $(0.68155, 0.68159)$ for the case $k = 4$. Accordingly, $\theta_{j,k=2} = 0.79696(2)$, $\theta_{j,k=3} = 0.72109(2)$, and $\theta_{j,k=4} = 0.68157(2)$.

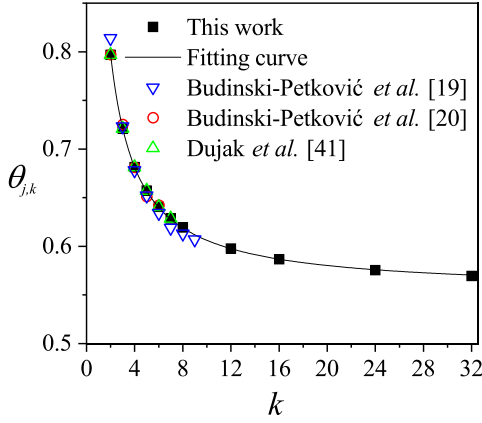


FIG. 5. Jamming coverage $\theta_{j,k}$ as a function of k for k -tiles on triangular lattices with k between 2 and 32 (solid squares). The size of the points is larger than the corresponding error bars. Down triangles, circles, and up triangles represent data obtained by Budinski-Petković and Kozmidis-Luburić [19], Budinski-Petković *et al.* [20] and Dujak *et al.* [41], respectively. The solid line corresponds to the fitting function as discussed in the text.

Following the procedure in Fig. 4, the jamming coverage was obtained for k ranging between 2 and 32. The results are shown in Fig. 5 (solid squares) together with the values reported by Budinski-Petković and Kozmidis-Luburić [19] (down triangles), Budinski-Petković *et al.* [20] (circles), and Dujak *et al.* [41] (up triangles). Clearly, the agreement between our results and those previously reported in the literature is excellent. For a more careful comparison, the values plotted in Fig. 2 are compiled in Table I. Small deviations are observed in the data from Ref. [19], which can be attributed to the small size of the lattice used in the calculations ($L = 128$ in Ref. [19]).

From $k \geq 2$ the data have been fitted to the function, $\theta_{j,k} = A + B/k + C/k^2$, as proposed in Ref. [44]; it is found that $A =$

$\theta_{j,k=\infty} = 0.5540(4)$, $B = 0.530(3)$, and $C = -0.084(2)$. The adjusted coefficient of determination is $R^2 = 0.99997$. The value $\theta_{j,k=\infty} = 0.5540(4)$ represents the limit concentration by infinitely large k -tiles.

As in the case of linear k -mers on triangular lattices [23], the jamming coverage of k -tiles on triangular lattices shows a decreasing function with k . However, the $\theta_{j,k=\infty} = 0.5540(4)$ for k -tiles is less than the value $\theta_{j,k=\infty} = 0.5976(5)$ obtained for linear k -mers on triangular lattices [23]. It means that linear k -mers are more effective in filling the lattice than k -tiles. The same behavior was observed for square lattices, where $\theta_{j,k=\infty} = 0.660(2)$ for linear k -mers [44] and $\theta_{j,k=\infty} = 0.5623(3)$ for square k -tiles [35].

In the case of objects removed from an initially fully occupied lattice, the removal process is equivalent to a standard RSA process in a complementary lattice. Accordingly, standard and inverse problems share formal aspects, terminology, and essential characteristics, such as the existence of a nontrivial state, the jammed saturation state. In fact, let us consider the complementary lattice to the original lattice, where each empty (occupied) site of the original lattice transforms into a occupied (empty) one of the complementary lattice. Under these conditions, the filling process in the complementary lattice (dilution process in the original lattice) is equivalent to a RSA process. Then, it is straightforward that $\theta_{j,k}^i = 1 - \theta_{j,k}$, where $\theta_{j,k}^i$ is the inverse jamming coverage corresponding to the removal process. In the present case, $\theta_{j,k}^i$ can be written as $\theta_{j,k}^i = 0.4460 - 0.530/k + 0.084/k^2$ ($k \geq 2$). Given that the inverse jamming coverage is exactly equal to one minus the standard jamming coverage, the values of $\theta_{j,k}^i$ are not shown in Fig. 5 (nor are they listed in Table I).

C. Percolation properties

Standard and inverse percolation thresholds can be calculated by using an extrapolation method based on scaling

TABLE I. The table compiles the numerical values of $\theta_{j,k}$, $\theta_{c,k}$, and $\theta_{c,k}^i$ obtained in the present work and in previous studies. Statistical errors are in the last digit and are indicated in parentheses. Values marked with asterisks were digitized from Refs. [19,20].

Isotropic case							
k	Standard model				Inverse model		
	$\theta_{j,k}$ (jamming)				$\theta_{c,k}$ (percolation)		$\theta_{c,k}^i$ (inverse percolation)
	Ref. [19]	Ref. [20]	Ref. [41]	This work	Ref. [41]	This work	This work
2	0.8139(1)	0.7970 (4)	0.7970(4)	0.79696(2)	0.5214(9)	0.52487(3)	0.47513(3)
3	0.723*	0.725*	0.7211(5)	0.72109(2)	0.5524(14)	0.55313(4)	0.44684(3)
4	0.678*	0.681*	0.6816(6)	0.68157(2)	0.5789(15)	0.57984(2)	0.42017(3)
5	0.652*	0.651*	0.6572(6)	0.65730(3)	0.6003(15)	0.60348(2)	0.39695(4)
6	0.634*	0.642*	0.6406(8)	0.64066(2)		0.62207(4)	0.37794(2)
7	0.619*		0.6286(7)	0.62865(3)			
8	0.613*			0.61945(2)			
9	0.607*						
12				0.59768(2)			
16				0.58677(2)			
24				0.57547(3)			
32				0.56965(3)			

laws [1]:

$$\theta_{c,k}(L) = \theta_{c,k} + A_k L^{-1/\nu}, \quad (1)$$

and

$$\theta_{c,k}^i(L) = \theta_{c,k}^i + A_k^i L^{-1/\nu}, \quad (2)$$

where $\theta_{c,k}$ [$\theta_{c,k}^i$] is the standard (inverse) percolation threshold in the thermodynamic limit ($L \rightarrow \infty$) for a tile of side k ; A_k and A_k^i are nonuniversal constants and ν is the critical exponent of the correlation length. As will be shown in Sec. IV B, the values of the critical exponents characterizing the percolation phase transition occurring in our model are consistent with those of 2D random percolation: $\nu = 4/3$, $\gamma = 43/18$, and $\beta = 5/36$ [1]. The quantities $\theta_{c,k}(L)$ [$\theta_{c,k}^i(L)$] represent the percolation thresholds for finite lattices.

A standard method to obtain $\theta_{c,k}(L)$ [$\theta_{c,k}^i(L)$] consists of the following steps: (a) the construction of a triangular lattice of linear size L and coverage θ , and (b) the cluster analysis using the Hoshen and Kopelman algorithm [45]. A total of r independent runs of such two steps procedure are carried out for each lattice size L and size k . From these runs, a number r^* of them present a percolating cluster. Then, a percolation probability can be defined as $R_{L,k}(\theta) = r^*/r$. In the present study, periodic boundary conditions are used to determine the percolation quantities.

In the case of standard (inverse) percolation problem, $R_{L,k}(\theta)$ represents the probability that a lattice of side L percolates at the concentration θ by the deposition (after the removal) of k -tiles [46]. $R_{L,k}^X(\theta)$ is an increasing (decreasing) sigmoid function of the coverage, and $\theta_{c,k}(L)$ [$\theta_{c,k}^i(L)$] can be obtained from the position of the inflection point of the function $R_{L,k}(\theta)$.

Different connectivity criteria (denoted by the index X) can be used to calculate $R_{L,k}(\theta)$ [46]:

- (1) $R_{L,k}^{X=R}(\theta)$: the probability of finding a rightward percolating cluster [see Fig. 1];
- (2) $R_{L,k}^{X=D}(\theta)$: the probability of finding a downward percolating cluster [see Fig. 1];
- (3) $R_{L,k}^{X=U}(\theta)$: the probability of finding a cluster which percolates in any direction;
- (4) $R_{L,k}^{X=I}(\theta)$: the probability of finding a cluster which percolates in both (mutually perpendicular) directions;
- (5) $R_{L,k}^{X=A}(\theta) = \frac{1}{2}[R_{L,k}^U(\theta) + R_{L,k}^I(\theta)]$.

In our percolation simulations, we used $r = 10^5$ independent random samples. In addition, for each value of k , the effect of finite size was investigated by examining different lattice sizes. As in previous section, we study lattices with k ranging between $k = 2$ and $k = 32$: $k = 2-8$, $L = 128-640$; and $k = 12-32$, $L = 256-1280$. From this analysis, finite-scaling theory can be used to determine the percolation threshold and the critical exponents with reasonable accuracy.

The percolation order parameter P and its corresponding susceptibility χ have been obtained from the largest cluster [47,48]:

$$P = \frac{\langle S_L \rangle}{M}, \quad (3)$$

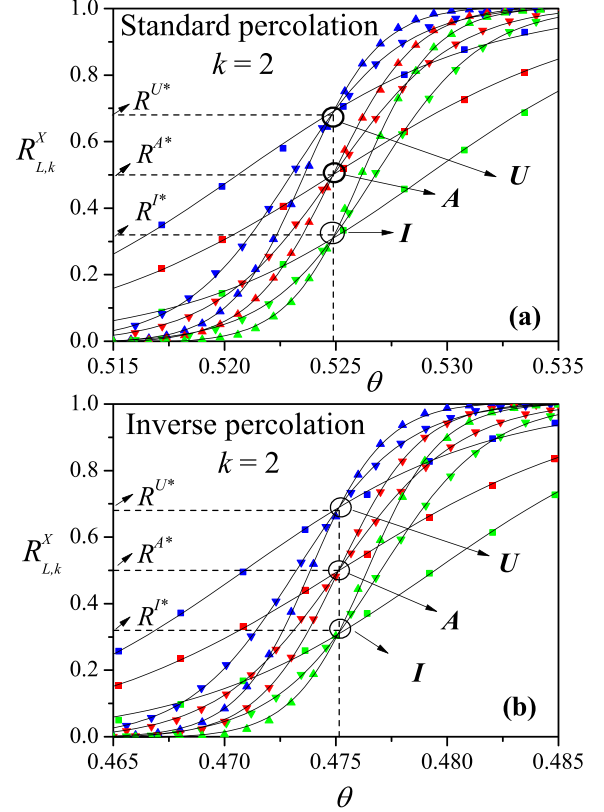


FIG. 6. Fraction of percolating lattices $R_{L,k}^X(\theta)$ ($X = \{I, U, A\}$, as indicated) as a function of the concentration θ for $k = 2$ and three different lattice sizes: $L = 128$, squares; $L = 384$, down triangles; and $L = 640$, up triangles. Symbols represent simulation results and solid lines correspond to fitting curves using the error function. The statistical errors are smaller than the symbol sizes. The curves in panel (a) [(b)] correspond to standard (inverse) percolation. The vertical dashed line denotes the percolation threshold in the thermodynamic limit.

and

$$\chi = \frac{[\langle S_L^2 \rangle - \langle S_L \rangle^2]}{M}, \quad (4)$$

respectively. The reduced fourth-order cumulant U_L introduced by Binder [49] was also calculated:

$$U_L = 1 - \frac{\langle S_L^4 \rangle}{3\langle S_L^2 \rangle^2}. \quad (5)$$

In Eqs. (3)–(5), $\langle \dots \rangle$ means an average over simulation runs,

In Fig. 6, the probabilities $R_{L,k}^A(\theta)$, $R_{L,k}^I(\theta)$, and $R_{L,k}^U(\theta)$ are presented for $k = 2$: (a) standard percolation and (b) inverse percolation. As mentioned above, the simulations were performed for lattice sizes ranging between $L = 128$ and $L = 640$. For clarity, simulation results from only three lattice sizes are shown in the figure: $L = 128$ (squares), $L = 384$ (down triangles), and $L = 640$ (up triangles). The solid lines correspond to fitting curves using the error function (see discussion in the next paragraph). The behavior of the probability curves $R_{L,k}^X(\theta)$ strongly depend on the system size. Even so, for a given criterion X , they all cross in a unique point R^{X*} . In this case, the obtained values $R^{A*} \approx 0.50$, $R^{I*} \approx 0.32$, and

$R^{U*} \approx 0.68$ agree (within the numerical errors) with the corresponding exact values for standard percolation: A criterion, $1/2$ [50,51]; I criterion, $0.322\ 120\ 45\dots$ [51,52], and U criterion, $0.677\ 889\ 54\dots$ [51,52]. In addition, the intersection points do not modify their numerical value for the different k -sizes studied (data not shown here for the sake of brevity). This finding represents a first indication that the phase transition involved in the standard and inverse percolation problem of triangular k -tiles on triangular lattices belongs to the ordinary percolation universality class no matter the value of k considered in the experiment.

As mentioned above, the values of $\theta_{c,k}(L)$ [$\theta_{c,k}^i(L)$] can be obtained from the positions of the inflection point of the probability functions. To do this, first it is convenient to fit the probability curves with some function through the least-squares method so that they can be expressed as a continuous function of θ . The fitting curve used is the *error function* because $dR_{L,k}^X(\theta)/d\theta$ is expected to behave like the Gaussian distribution near the peak. This assumption is good enough to obtain the parameters that are needed to apply finite-size scaling theory [1,53],

$$\frac{dR_{L,k}^X(\theta)}{d\theta} = \frac{1}{\sqrt{2\pi}\Delta_{L,k}^X} \exp\left\{-\frac{1}{2}\left[\frac{\theta - \theta_{c,k}^X(L)}{\Delta_{L,k}^X}\right]^2\right\}, \quad (6)$$

where $\theta_{c,k}^X(L)$ is the concentration at which the slope of $R_{L,k}^X(\theta)$ is the largest and $\Delta_{L,k}^X$ is the standard deviation from $\theta_{c,k}^X(L)$.

Figure 7 shows the plots towards the thermodynamic limit of the standard [Fig. 7(a)] and inverse [Fig. 7(b)] percolation thresholds according to Eqs. (1) and (2) for the data in Fig. 6. The critical exponent ν was set as $\nu = 4/3$ for the present analysis, since, as will be shown in Sec. IV, our model belongs to the same universality class as random percolation [1]. From extrapolations it is possible to obtain $\theta_{c,k}^X(\infty)$ [$\theta_{c,k}^{i,X}(\infty)$] for the criteria I , A , and U . Combining the three estimates for each case, the final values of $\theta_{c,k}(\infty)$ [$\theta_{c,k}^i(\infty)$] can be obtained. The maximum of the differences between $|\theta_{c,k}^U(\infty) - \theta_{c,k}^A(\infty)|$ [$|\theta_{c,k}^{i,U}(\infty) - \theta_{c,k}^{i,A}(\infty)|$] and $|\theta_{c,k}^I(\infty) - \theta_{c,k}^A(\infty)|$ [$|\theta_{c,k}^{i,I}(\infty) - \theta_{c,k}^{i,A}(\infty)|$] gives the error bar for each determination of $\theta_{c,k}(\infty)$ [$\theta_{c,k}^i(\infty)$]. In this case, the values obtained were $\theta_{c,k=2}(\infty) = 0.524\ 87(3)$ and $\theta_{c,k=2}^i(\infty) = 0.475\ 13(3)$. For the rest of the paper, we denote the standard and inverse percolation thresholds for each size k by $\theta_{c,k}$ and $\theta_{c,k}^i$, respectively [for simplicity we drop the symbol “ (∞) ”].

By following the procedure of Fig. 7, standard and inverse percolation thresholds were calculated for different values of k . The results are collected in Fig. 8: solid black circles and open red circles represent standard and inverse percolation thresholds for k -tiles on triangular lattices, respectively. For comparison, the figure includes the values of the standard percolation thresholds obtained by Dujak *et al.* [41] (open triangles). The figure also shows the jamming curves corresponding to standard ($\theta_{j,k}$ vs k , solid squares) and inverse ($\theta_{j,k}^i$ vs k , open squares) problems. Open and solid circles represent data obtained in this work. Open triangles correspond to data obtained by Dujak *et al.* [41]. The curves were obtained by following the isotropic deposition-removal scheme. The dotted lines are simply a guide for the eye.

In the case of standard percolation, $\theta_{c,k}$ is a monotonically increasing function of k in the interval [1,6]. However, when

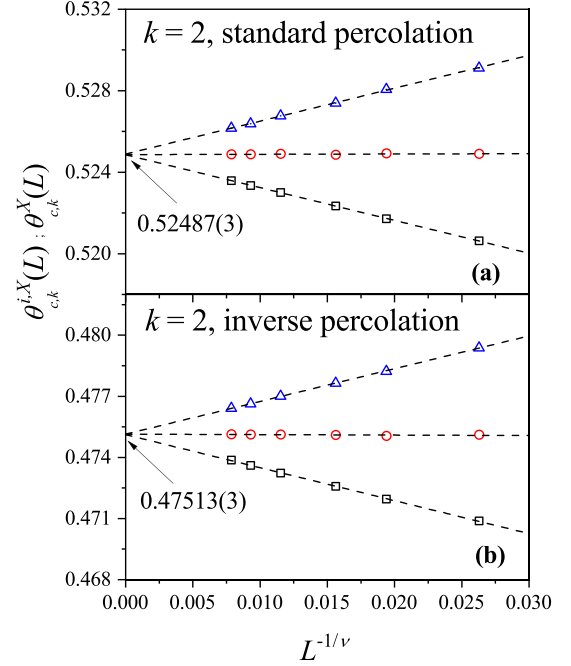


FIG. 7. Extrapolation of the standard [panel (a)] and inverse [panel (b)] percolation thresholds toward the thermodynamic limit according to the theoretical predictions given by Eqs. (1) and (2). The values presented in the figure were obtained for $k = 2$. Squares, circles, and triangles denote the values of $\theta_{c,k}^X(L)$ [$\theta_{c,k}^{i,X}(L)$] obtained by using the criteria I , A , and U , respectively. The bar error in each measurement is smaller than the size of the corresponding symbol.

k increases above six ($k \geq 7$), all jammed configurations are nonpercolating states, and consequently, there is no percolating phase. This phenomenon can be better understood by examining Fig. 9, where the curves of $R_{L,k}^X(\theta)$ ($X = I, U, A$

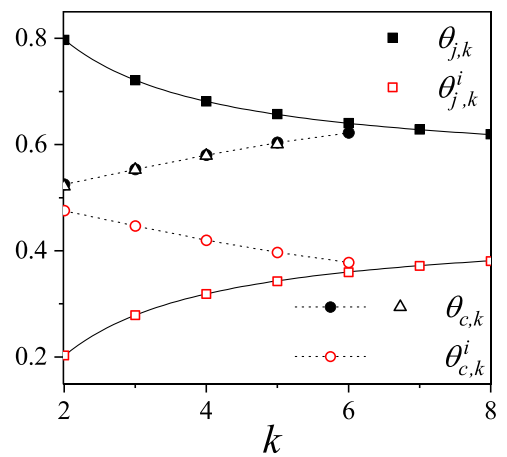


FIG. 8. Standard (solid circles and open triangles) and inverse (open circles) percolation thresholds for k -tiles on triangular lattices. The figure also includes the jamming data corresponding to standard (solid squares and solid line) and inverse (open squares and solid lines) problems. Open and solid circles represent data obtained in this work. Open triangles correspond to data obtained by Dujak *et al.* [41]. The curves were obtained by following the isotropic deposition-removal scheme. The dotted lines are simply a guide for the eye.

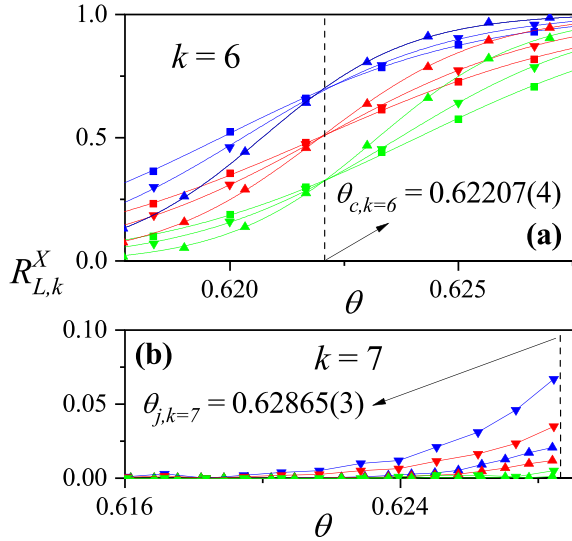


FIG. 9. (a) Fraction of percolating lattices $R_{L,k}^X(\theta)$ as a function of the concentration θ for the isotropic case, $k = 6$ and different lattice sizes: $L = 128$ (squares), 192 (down triangles), and 384 (up triangles). Blue, red, and green symbols represent data for U , A , and I criteria, respectively. Dashed line denotes the percolation threshold in the thermodynamic limit $L \rightarrow \infty$, respectively. (b) Same as panel (a) but for $k = 7$. For clarity, only the curves for $L = 192$ (down triangles) and $L = 384$ (up triangles) are plotted. The vertical dashed line indicates the jamming coverage.

as indicated) as a function of the concentration θ are shown for $k = 6$ [Fig. 9(a)] and $k = 7$ [Fig. 9(b)]. Three lattice sizes are shown for $k = 6$: $L = 128$ (squares), $L = 192$ (down triangles), and $L = 384$ (up triangles). In the case of $k = 7$, only the curves for $L = 192$ (down triangles) and $L = 384$ (up triangles) are plotted.

For $k = 6$, the probabilities $R_{L,k}^A(\theta)$, $R_{L,k}^I(\theta)$, and $R_{L,k}^U(\theta)$ look similar to those of Fig. 6. Namely, the curves for different lattice sizes cross each other in a unique point (which depends on the criterion X used), determining the percolation threshold in the thermodynamic limit. In this case, $\theta_{c,k=6} = 0.62207(4)$. The situation is different for $k = 7$, where the curves of $R_{L,k}^X(\theta)$ remain almost constant and close to zero up to the jamming coverage $\theta_{j,k=6} = 0.62865(3)$ (vertical dashed line in the figure). This finding is a clear indication that (i) the percolation phase transition disappears, and (ii) there is only one phase (the nonpercolating phase) for $k > 6$.

The interplay between the percolation and the jamming effects is responsible for the existence of a maximum value of k (in this case, $k_{\max} = 6$) from which the percolation phase transition no longer occurs. In fact, as established in Ref. [42], different behaviors can be observed depending on the relationship between the dimension of the deposited object and the dimension of the substrate. When the dimension of the lattice is the same as the dimension of the depositing object, which is the case considered here, the percolation threshold is an increasing function of the size k in the range ($k \leq k_{\max}$) and, for $k > k_{\max}$, the percolation phase transition disappears. Thus, (1) $k_{\max} = 1$ for straight rigid k -mers on one-dimensional (1D) lattices [1,5]; (2) $k_{\max} = 3$ for $k \times k$ square tiles (k^2 -mers) on 2D square lattices [33–35]; (3)

$k_{\max} = 16$ for $k \times k \times k$ cubic objects (k^3 -mers) deposited on three-dimensional (3D) simple cubic lattices [42]; and (4) $k_{\max} = 6$ for k -tiles on 2D triangular lattices (this work).

Returning to Fig. 8, a good agreement is obtained between our results and those of Dujak *et al.* [41] in the interval $k = 2$ –5. For $k = 6$, no percolation was found in Ref. [41]. This was possibly due to the fact that the difference between $\theta_{j,k=6}$ and $\theta_{c,k=6}$ is very small, which makes it difficult to calculate percolation properties.

In the case of inverse percolation (open red circles in Fig. 8), $\theta_{c,k}^i$ is a decreasing function of k in the range $2 \leq k \leq 6$. For $k \geq 7$, all jammed configurations are percolating states (the lattice remains connected even when the highest allowed concentration of removed sites is reached) and, consequently, there is no nonpercolating phase. As shown in the figure, a complementarity property between the percolation thresholds for standard and inverse percolation is found: $\theta_{c,k} + \theta_{c,k}^i = 1$. This property, which has also been observed for linear k -mers on triangular lattices [26], is exact for the case $k = 1$ [1] and it holds for the entire range of k where the percolation phase transition exists. For each k , $\theta_{c,k} + \theta_{c,k}^i = 1$ within the numerical error (see Table I). The complementarity property is a typical property of the triangular lattice [54,55] and it is not observed in other geometries, such as square [30,33–35,40,56] or honeycomb lattices [57,58].

III. STANDARD AND INVERSE PERCOLATION OF PERFECTLY ORIENTED k -TILES ON TRIANGULAR LATTICES

To have a more complete insight of the percolation processes of k -tiles on the triangular lattice, in this section, the oriented percolation is studied with a focus in the complementary property observed in the isotropic case.

A. Model and basic definitions

To study the effect of k -tile alignment on percolation, the deposition process is performed as in Sec. II A but, now, the following restriction is considered: the k -tiles are attempted to be deposited only in the up direction [s_1 structure in Fig. 2(a)]. This leads to the formation of an oriented structure as depicted in Fig. 10(a). Periodic boundary conditions are considered in the deposition procedure.

To distinguish between isotropic and oriented problem, for the rest of the paper we use the variable ϑ to denote the concentration of occupied sites for the case of perfectly oriented deposition. It is important to note that, in the present paper, we treat with completely aligned states generated by irreversible adsorption of k -tiles. This phenomenon should not be confused with the classical nematic condition occurring in thermodynamic equilibrium. Interesting examples of equilibrium ordered states of k -tiles with $k = 2$ can be found in Ref. [59].

The inverse percolation problem is also considered for the case of perfectly oriented k -tiles in the up direction. We start from an initially fully occupied lattice, where all lattice sites are occupied by single monomers (each monomer occupies one lattice site). The full occupation state is diluted as follows: (1) set of $k(k+1)/2$ sites forming a up k -tile is

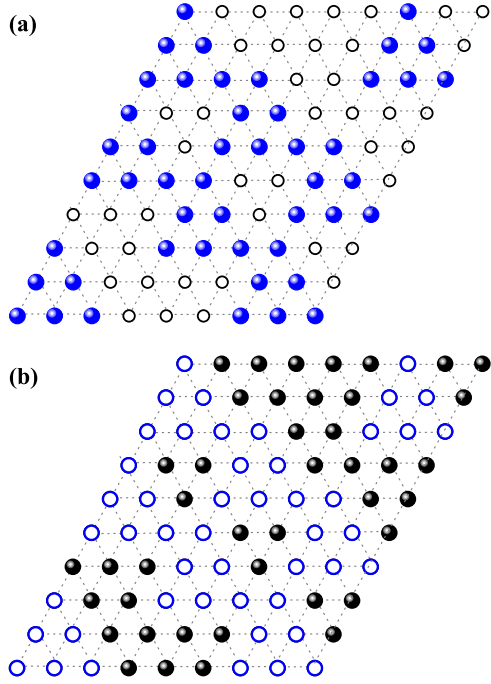


FIG. 10. (a) Schematic representation of a typical configuration obtained by deposition of 3-tiles perfectly oriented in the up direction (up 3-tiles). Solid spheres represent the units (monomers) belonging to the deposited up 3-tiles, and open circles correspond to empty sites. (b) Schematic representation of a typical configuration obtained by removing up 3-tiles from an initially fully occupied portion of lattice. Solid spheres represent occupied sites (monomers), and open circles indicate empty sites resulting from the removal of the up 3-tiles.

chosen at random; and (2) if the $k(k + 1)/2$ sites selected in step (1) are occupied, then an up k -tile is removed from those sites. Otherwise, the attempt is rejected. Steps (1) and (2) are repeated until the desired number of k -tiles N is removed from the lattice and the concentration of occupied particles is $\vartheta^i = [M - k(k + 1)N/2]/M$. The removal process leads to configurations as depicted in Fig. 10(b). Periodic boundary conditions are considered.

B. Jamming properties

Following the procedure used for the isotropic case (see Fig. 4), the jamming thresholds were determined from the intersection points of the probability curves $W'_{L,k}(\vartheta)$ for different values of L (these data are not shown here for brevity). The values of n , k , and L used in the simulations were the same as those in Sec. II B: $n = 2 \times 10^4$; $k = 2-8$, $L = 128-640$; and $k = 12-32$, $L = 256-1280$. The results are shown in Fig. 11 (solid diamonds) and compiled in Table II.

As can be observed from Fig. 11, $\vartheta_{j,k}$ monotonically decrease with increasing k . From $k \geq 2$, the data can be well fitted by the function $\vartheta_{j,k} = A + B/k + C/k^2$, with $A = \vartheta_{j,k=\infty} = 0.36619(8)$, $B = 0.5565(8)$, and $C = 0.199(2)$. The adjusted coefficient of determination is $R^2 = 0.99998$. The limit jamming $\vartheta_{j,k=\infty} = 0.36619(8)$ is less than the value $\theta_{j,k=\infty} = 0.5540(4)$ obtained for the isotropic case. These results are qualitatively different from those

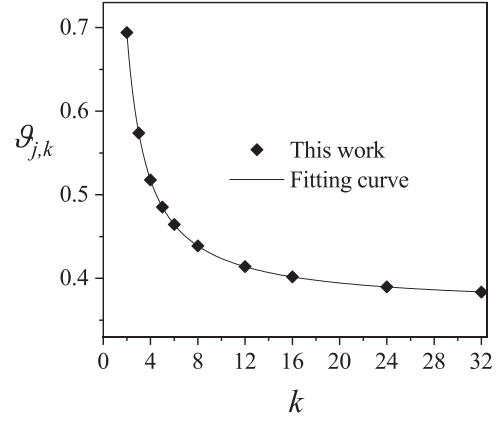


FIG. 11. Jamming coverage $\vartheta_{j,k}$ as a function of k for perfectly oriented k -tiles on triangular lattices with k between 2 and 32 (solid diamonds). The size of the points is larger than the corresponding error bars. The solid line corresponds to the fitting function as discussed in the text.

obtained for straight rigid k -mers, where the limit jamming for isotropic straight rigid k -mers is less than the limit jamming for aligned straight rigid k -mers: $\theta_{j,k=\infty} = 0.660(2)$ [44] and $\vartheta_{j,k=\infty} = 0.7475979202$ [60] for square lattices; and $\theta_{j,k=\infty} = 0.5976(5)$ [23] and $\vartheta_{j,k=\infty} = 0.7475979202$ [60] for triangular lattices.² Clearly, the structure of the lattice plays a fundamental role in determining the statistics and percolation properties of extended objects.

Finally, the jamming coverage for the inverse problem $\vartheta_{j,k}^i$ can be written as $\vartheta_{j,k}^i = 1 - \vartheta_{j,k}$. Then, $\vartheta_{j,k}^i = 0.63381 - 0.5565/k - 0.199/k^2$ ($k \geq 2$).

²For a 2D system of aligned straight rigid k -mers, the rods are deposited only along an axis of the lattice, and the jamming problem (independently of the lattice geometry) reduces to the one-dimensional (1D) case. In this limit, the jamming coverage for infinitely long rods ($k \rightarrow \infty$) tends to the Rényi's parking constant $c_R \approx 0.7475979202$ [60].

TABLE II. The table compiles the numerical values of $\vartheta_{j,k}$, $\vartheta_{c,k}$, and $\vartheta_{c,k}^i$ obtained in the present work. Statistical errors are in the last digit and are indicated in parentheses.

k	Nematic case		
	Standard model		Inverse model
	$\vartheta_{j,k}$ (jamming)	$\vartheta_{c,k}$ (percolation)	$\vartheta_{c,k}^i$ (inverse percolation)
2	0.69412(1)	0.49854(2)	0.50147(3)
3	0.57393(1)	0.50140(4)	0.49867(4)
4	0.51774(2)	0.50071(4)	0.49935(3)
5	0.48538(2)		
6	0.46440(2)		
8	0.43877(3)		
12	0.41391(2)		
16	0.40181(3)		
24	0.38985(3)		
32	0.38369(3)		

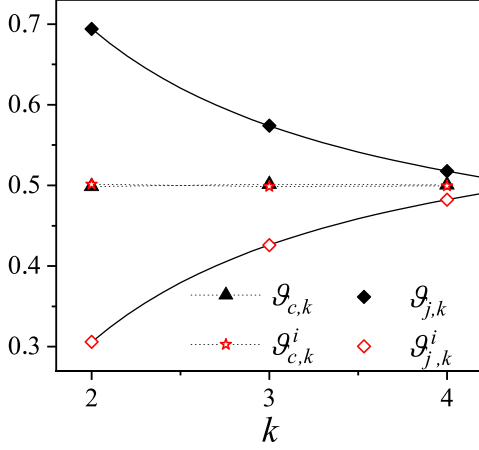


FIG. 12. Standard (solid triangles) and inverse (open stars) percolation thresholds for k -tiles on triangular lattices. The figure also includes the jamming data corresponding to standard (solid diamonds and solid line) and inverse (open diamonds and solid line) problems. The curves were obtained by following the nematic deposition-removal scheme. The dotted lines are simply a guide for the eye.

C. Percolation properties

The standard and inverse percolation thresholds are obtained through the extrapolation given by Eqs. (1) and (2). In this case, the equations can be written as

$$\vartheta_{c,k}(L) = \vartheta_{c,k} + \tilde{A}_k L^{-1/\nu}, \quad (7)$$

and

$$\vartheta_{c,k}^i(L) = \vartheta_{c,k}^i + \tilde{A}_k^i L^{-1/\nu}, \quad (8)$$

where \tilde{A}_k and \tilde{A}_k^i are the scaling constants for the standard and inverse perfectly oriented problem, respectively. Once the positions $\vartheta_{c,k}(L)$ and $\vartheta_{c,k}^i(L)$ are determined from the percolation probability functions $R_{L,k}(\vartheta)$, the percolation thresholds $\vartheta_{c,k}$ and $\vartheta_{c,k}^i$ can be obtained using the extrapolation scheme in Eqs. (7) and (8).

The results obtained for $\vartheta_{c,k}$ and $\vartheta_{c,k}^i$ as functions of size k are shown in Fig. 12 and collected in Table II. Solid triangles and open stars represent standard and inverse percolation thresholds, respectively. The behavior of $\vartheta_{c,k}$ and $\vartheta_{c,k}^i$ in terms of k is reported here. Figure 12 includes the jamming curves corresponding to standard ($\vartheta_{j,k}$ vs k , solid diamonds) and inverse ($\vartheta_{j,k}^i$ vs k , open diamonds) problems.

The behavior of $\vartheta_{c,k}$ ($\vartheta_{c,k}^i$) is similar to that obtained for isotropic deposition (removal), see Fig. 8. In this case, $k_{\max} = 4$. For $k > 4$, the percolation phase transition disappears. In addition, the values of standard and inverse percolation thresholds are symmetric to each other with respect to the line $\vartheta = 0.5$. Thus, as in the isotropic percolation problem, $\vartheta_{c,k} + \vartheta_{c,k}^i = 1$ within the numerical error and, accordingly, the complementarity property is also valid for the perfectly oriented percolation problem.

Finally, it is interesting to analyze the inverse percolation problem in terms of robustness. The focus of robustness in complex networks is the response of the network to the removal of nodes or links [9–12]. Combining the percolation (in

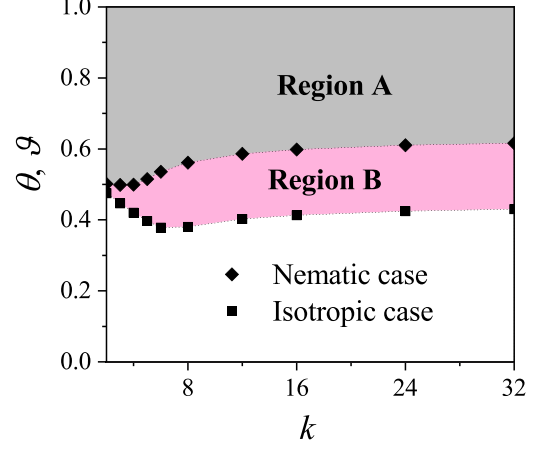


FIG. 13. The figure shows the boundary curves separating percolating and nonpercolating or forbidden regions for inverse percolation of k -tiles on triangular lattices. Solid squares and solid diamonds correspond to isotropic and nematic model, respectively. Accordingly, region A (region A and region B) represents the percolating area for the nematic (isotropic) removal scheme.

the range $2 \leq k \leq k_{\max}$) and jamming (in the range $k > k_{\max}$) thresholds, the boundary curves separating percolating and nonpercolating or forbidden regions can be constructed. The results of this procedure are shown in Fig. 13 for inverse percolation and isotropic (solid squares) and nematic (solid diamonds) removal scheme. As can be observed from the figure, the percolating area for the isotropic case (region A and region B) is larger than the corresponding percolating area for the nematic case (region A). This means that the phase of occupied sites is more robust when the k -tiles are removed isotropically. A contrary behavior has been observed for inverse percolation of straight rigid k -mers on triangular lattices [26], where the boundary curve for isotropic percolation is above the oriented one in the whole range of k . In this case, it is easier to disconnect the system when the needles are isotropically removed. In other words, the system is more robust when the removed needles are aligned in only one direction.

IV. CRITICAL EXPONENTS AND UNIVERSALITY

In this section, the critical exponents corresponding to jamming and percolation problems will be calculated. In the first case, the jamming exponent ν_j will be obtained from the probability curves $W'_{L,k}$. In the second case, the complete set of static critical exponents will be determined from the scaling behavior of the curves of percolation probability $R'_{L,k}(\nu)$, order parameter $P(\beta)$, and susceptibility $\chi(\gamma)$. Knowing ν , β , and γ is enough to characterize the universality class of our system and understand the related phenomena.

A. Jamming critical exponent

The critical exponent ν_j of the jamming transition was obtained for the isotropic and nematic cases. As discussed in Sec. II B, the quantity $W'_{L,k} = 1 - W_{L,k}$ can be fitted by the error function. Thus, $dW'_{L,k}/dx$ ($x = \theta$ for the isotropic case and $x = \vartheta$ for the nematic case) is expected to behave like the

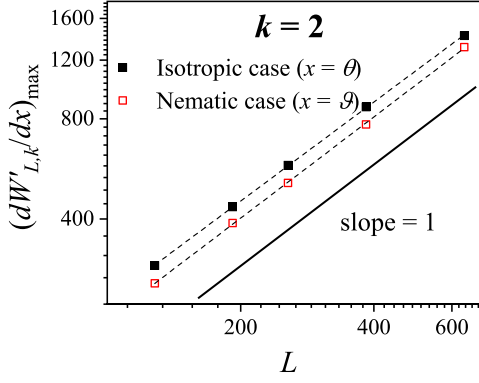


FIG. 14. $\log_{10}\text{-}\log_{10}$ plot of $(dW'_{L,k}/dx)_{\max}$ as a function of L for two different cases: $k = 2$ and isotropic problem ($x = \theta$, solid squares); and $k = 2$ and nematic problem ($x = \vartheta$, open squares). According to Eq. (10) the slope of the line corresponds to $1/\nu_j$. In this case, $\nu_j = 1.01(2)$ (isotropic problem) and $\nu_j = 0.99(2)$ (nematic problem).

Gaussian distribution [53],

$$\frac{dW'_{L,k}}{dx} = \frac{1}{\sqrt{2\pi}\Delta'_{L,k}} \exp\left\{-\frac{1}{2}\left[\frac{x - x_{j,k}(L)}{\Delta'_{L,k}}\right]^2\right\}, \quad (9)$$

where $x_{j,k}(L)$ is the concentration at which the slope of $dW'_{L,k}/dx$ is the largest and $\Delta'_{L,k}$ is the standard deviation from $x_{j,k}(L)$.

Then, ν_j can be calculated from the maximum of the derivative of $W'_{L,k}$:

$$\left(\frac{dW'_{L,k}}{dx}\right)_{\max} \propto L^{1/\nu_j}. \quad (10)$$

If $(dW'_{L,k}/dx)_{\max}$ is plotted as a function of L in $\log_{10}\text{-}\log_{10}$ scale, the slope of the line will correspond to $1/\nu_j$. Figure 14 shows $\log_{10}[(dW'_{L,k}/dx)_{\max}]$ as a function of $\log_{10} L$ for $k = 2$ and isotropic ($x = \theta$, solid squares) and nematic ($x = \vartheta$, open squares) cases. Then, ν_j can be obtained from the inverse of the slope of the line. In the cases of Fig. 14, $\nu_j = 1.01(2)$ (isotropic problem) and $\nu_j = 0.99(2)$ (nematic problem).

The procedure was repeated for different values of k . The results are shown in Table III. In all the cases, the values obtained for ν_j (1) remain close to 1, and (2) coincide, within the numerical errors, with the values previously reported in other 2D monolayer systems [34,35,40,61].

As shown in previous, the properties of $W'_{L,k}$ are identical to those of $R_{L,k}^X$ in standard percolation transitions. Namely, $R_{L,k}^X$ obeys the same scaling relation in Eq. (10), and the intersection of the curves of $R_{L,k}^X$ for different system sizes can be used to determine the critical point that characterizes the percolation transition occurring in the system. Then, based on these features, we propose the following scaling behavior at criticality for the probability $W'_{L,k}$:

$$W'_{L,k}(x) = \overline{W}'_k[(x - x_{j,k})L^{1/\nu_j}], \quad (11)$$

where \overline{W}'_k is the corresponding scaling function and as established above, $x = \theta$ for the isotropic case and $x = \vartheta$ for the nematic case.

TABLE III. The table compiles the numerical values of the jamming critical exponent ν_j obtained in the present work. Statistical errors are in the last digit and are indicated in parentheses.

Jamming critical exponent ν_j		
k	Isotropic model	Nematic model
2	1.01(2)	0.99(2)
3	0.99(2)	1.00(2)
4	1.01(2)	0.99(2)
5	0.99(2)	1.02(2)
6	1.01(1)	1.00(1)
8	0.99(2)	0.99(2)
12	1.00(2)	0.99(2)
16	1.00(2)	1.01(2)
24	1.01(2)	1.00(3)
32	1.00(2)	0.98(3)

The scaling tendency in Eq. (11) has been tested by plotting $W'_{L,k}(x)$ versus $(x - x_{j,k})L^{1/\nu_j}$ and looking for data collapsing. As an example, Fig. 15 shows the obtained results for $k = 2$ and isotropic [Fig. 15(a)] and nematic [Fig. 15(b)] cases. Using the values of $\theta_{j,k=2} = 0.79696(2)$, $\vartheta_{j,k=2} = 0.69412(1)$, and $\nu_j = 1$, the curves present an excellent scaling collapse. This data collapse study allows for consistency check of the value $\nu_j = 1$ calculated in Fig. 14.

B. Percolation critical exponents

To determine the universality class which this problem belongs to, the critical exponents ν , β , and γ have been calculated. As was done in previous section, and for a more compact notation, we define the generalized coverage x , which represents the percolation variable associated with each system studied. Thus, (i) $x = \theta$ for standard percolation and isotropic deposition model; (ii) $x = \vartheta$ for standard percolation

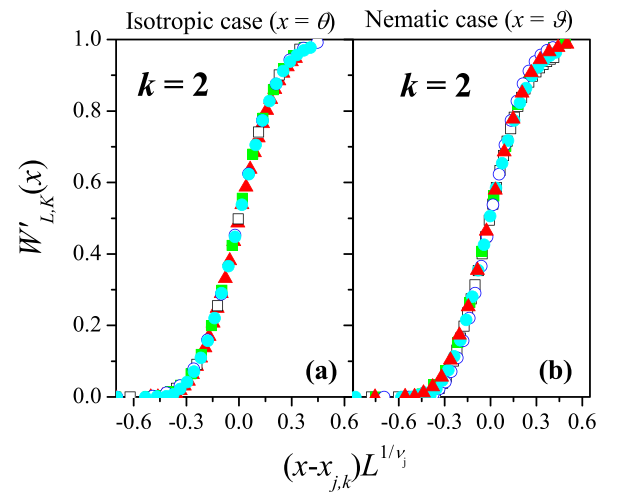


FIG. 15. (a) Data collapse of $W'_{L,k}(\theta)$ versus $(\theta - \theta_{j,k})L^{1/\nu_j}$ [Eq. (11)] for $k = 2$ and isotropic case. The curves were obtained using $\theta_{j,k=2} = 0.79696(2)$ and $\nu_j = 1$. (b) Same as in panel (a), but for nematic case. In this case, the curves were obtained using $\vartheta_{j,k=2} = 0.69412(1)$ and $\nu_j = 1$.

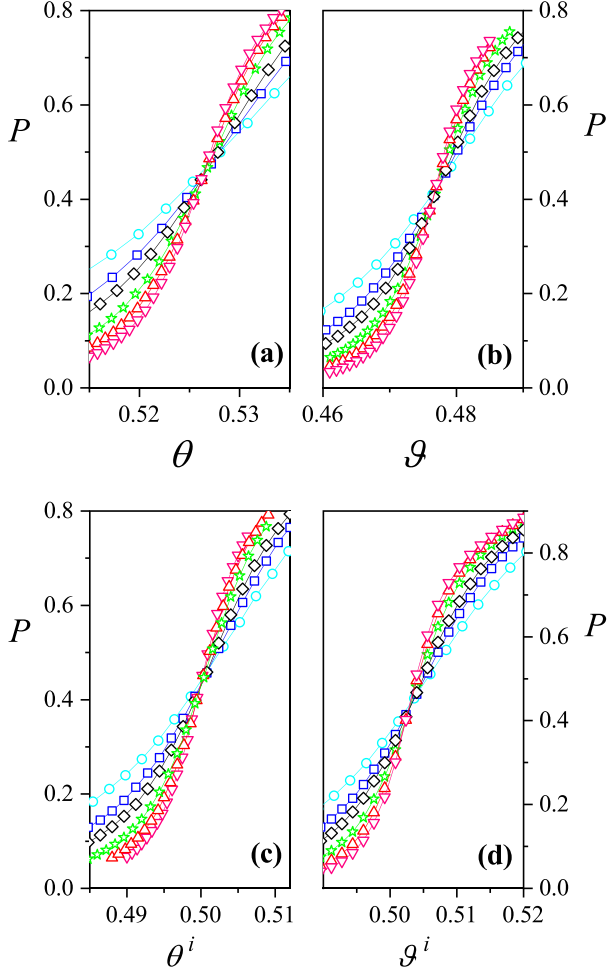


FIG. 16. Percolation order parameter P as a function of coverage x for $k = 2$ and four different cases: (a) standard percolation and isotropic deposition model ($x = \theta$); (b) standard percolation and nematic deposition model ($x = \vartheta$); (c) inverse percolation and isotropic removal model ($x = \theta^i$); and (d) inverse percolation and nematic removal model ($x = \vartheta^i$). Different symbols correspond to different lattice sizes: circles, $L = 128$; squares, $L = 192$; diamonds, $L = 256$; stars, $L = 384$; up triangles, $L = 512$; and down triangles, $L = 640$.

and nematic deposition model; (iii) $x = \theta^i$ for inverse percolation and isotropic removal model; and (iv) $x = \vartheta^i$ for inverse percolation and nematic removal model.

The strategy used to obtain the percolation critical exponents is based on the scaling properties of the percolation probability $R_{L,k}$ and the order parameter P (and its derivatives). Typical curves of $R_{L,k}$ versus coverage for different lattice sizes L are shown in Fig. 6. In the case of the order parameter, an illustrative example of the behavior of $P(x)$ for different values of L is presented in Fig. 16(a), standard percolation and isotropic deposition model, $x = \theta$; Fig. 16(b), standard percolation and nematic deposition model, $x = \vartheta$; Fig. 16(c), inverse percolation and isotropic removal model, $x = \theta^i$; and Fig. 16(d), inverse percolation and nematic removal model, $x = \vartheta^i$. Different symbols correspond with different lattice sizes: circles, $L = 128$; squares, $L = 192$; diamonds, $L = 256$; stars, $L = 384$; up triangles, $L = 512$;

and down triangles, $L = 640$. In all cases, the curves were obtained for $k = 2$.

According to scaling assumptions, the standard finite size scaling theory [47–49] provides several ways to estimate the critical exponent ν from simulation data. One of these methods is from the maximum of the function $dR_{L,k}^X/dx$,

$$\left(\frac{dR_{L,k}^X}{dx}\right)_{\max} \propto L^{1/\nu}. \quad (12)$$

In Fig. 17(a), $\log_{10}[(dR_{L,k}^A/dx)_{\max}]$ has been plotted as a function of $\log_{10} L$ (note the \log_{10} - \log_{10} functional dependence) for $k = 2$ and four different cases as indicated. According to Eq. (12), the slope of each line corresponds to $1/\nu$. As can be observed, the slopes of the curves remain constant, being $\nu = 1.334(9)$ for standard percolation and the isotropic deposition model; $\nu = 1.342(15)$ for standard percolation and the nematic deposition model; $\nu = 1.345(14)$ for inverse percolation and the isotropic removal model; and $\nu = 1.336(11)$ for inverse percolation and the nematic removal model.

Once ν was known, the exponent γ can be determined by scaling the maximum value of the susceptibility in Eq. (4). The behavior of χ at criticality is $\chi = L^{\gamma/\nu} \bar{\chi}(u)$, where $u = (x - x_{c,k})L^{1/\nu}$ and $\bar{\chi}$ is the corresponding scaling function. At the point where χ is maximal, $u = \text{const}$ and $\chi_{\max} \propto L^{\gamma/\nu}$. The data for χ_{\max} with $k = 2$ and the same cases in Fig. 17(a) are shown in Fig. 17(b). The values obtained are $\gamma = 2.40(2)$ for standard percolation and the isotropic deposition model; $\gamma = 2.40(2)$ for standard percolation and the nematic deposition model; $\gamma = 2.41(4)$ for inverse percolation and the isotropic removal model; and $\gamma = 2.41(3)$ for inverse percolation and the nematic removal model.

And finally, the exponent β can be determined from the scaling behavior at criticality of the order parameter in Eq. (3): $P = L^{-\beta/\nu} \bar{P}(u')$, where $u' = |x - x_{k,c}|L^{1/\nu}$ and \bar{P} is the scaling function. At the point where dP/dx is maximal, $u' = \text{const}$ and $(dP/dx)_{\max} = L^{(-\beta/\nu+1/\nu)} \bar{P}(u') \propto L^{(1-\beta)/\nu}$.

The scaling tendencies of $(dP/dx)_{\max}$ are shown in Fig. 17(c) for the same cases as in Figs. 17(a) and 17(b). From the slopes of the curves, the following values of β were obtained: $\beta = 0.131(9)$ for standard percolation and the isotropic deposition model; $\beta = 0.144(7)$ for standard percolation and the nematic deposition model; $\beta = 0.145(7)$ for inverse percolation and the isotropic removal model; and $\beta = 0.145(9)$ for inverse percolation and the nematic removal model.

The study carried out in Fig. 17 was repeated for all values of k where the percolation phase transition exists. For each k , the values of ν , γ , and β were determined from the corresponding linear regressions. The obtained results are compiled in Table IV. In all cases, these results are consistent (within the statistical error) with the exact values of the critical exponents of the ordinary percolation, $\nu = 4/3$, $\gamma = 43/18$, and $\beta = 5/36$.

Finally, the scaling behavior has also been tested by plotting $PL^{\beta/\nu}$ versus $|x - x_{k,c}|L^{1/\nu}$, $\chi L^{-\gamma/\nu}$ versus $(x - x_{k,c})L^{1/\nu}$, R_L^A versus $(x - x_{k,c})L^{1/\nu}$, and U versus $(x - x_{k,c})L^{1/\nu}$ and looking for data collapsing. Using the values

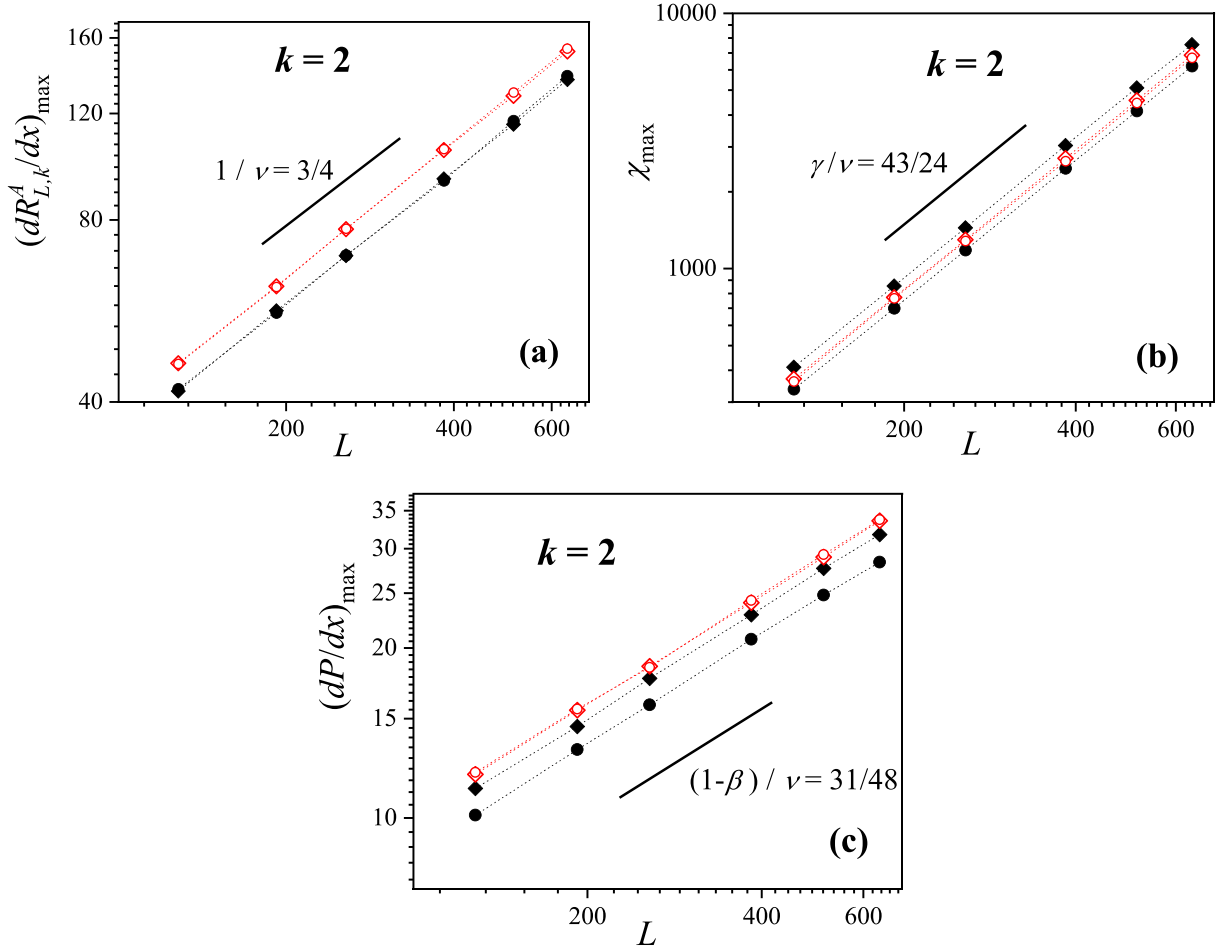


FIG. 17. (a) $\text{Log}_{10}\text{-log}_{10}$ plot of $(dR_{L,k}^A/dx)_{\max}$ as a function of L for $k = 2$ and four different cases: standard percolation and isotropic deposition model ($x = \theta$, solid diamonds); standard percolation and nematic deposition model ($x = \vartheta$, open diamonds); inverse percolation and isotropic removal model ($x = \theta^i$, solid circles); and inverse percolation and nematic removal model ($x = \vartheta^i$, open circles). According to Eq. (12), the slope of each line corresponds to $1/\nu = 3/4$. (b) $\text{Log}_{10}\text{-log}_{10}$ plot of χ_{\max} as a function of L for the cases in panel (a). The slope of each line corresponds to $\gamma/\nu = 43/24$. (c) $\text{Log}_{10}\text{-log}_{10}$ plot of $(dP/dx)_{\max}$ as a function of L for the same cases reported in panels (a) and (b). The slope of each line corresponds to $(1 - \beta)/\nu = 31/48$.

of $x_{k,c}$ calculated above and the exact values of the critical exponents corresponding to ordinary percolation $\nu = 4/3$, $\gamma = 43/18$, and $\beta = 5/36$, we obtain an excellent scaling collapse, as shown in Figs. 18 and 19 for $k = 2$ and different percolation criteria as indicated. This leads to independent

controls and consistency checks of the values of all the critical exponents.

It is well known that RSA has very short-range correlations which corroborated by the values of ν , γ , and β reported in previous paragraphs. This also means that the percolation

TABLE IV. The table compiles the numerical values of the percolation critical exponents ν , β , and γ obtained in the present work. Statistical errors are in the last digit and are indicated in parentheses.

k	Isotropic case						Nematic case					
	Standard model			Inverse model			Standard model			Inverse model		
	ν	β	γ	ν	β	γ	ν	β	γ	ν	β	γ
2	1.334(9)	0.131 (9)	2.40(2)	1.345(14)	0.145(7)	2.41(4)	1.342(15)	0.144(7)	2.40(2)	1.336(11)	0.145(9)	2.41(3)
3	1.339(8)	0.141 (8)	2.41(3)	1.341(10)	0.143(9)	2.41(3)	1.340(11)	0.139(7)	2.37(3)	1.341(10)	0.142(7)	2.39(3)
4	1.337(9)	0.137 (7)	2.39(4)	1.339(9)	0.142(8)	2.39(3)	1.338(11)	0.137(8)	2.41(4)	1.339(11)	0.140(8)	2.40(3)
5	1.336(9)	0.140 (9)	2.38(3)	1.342(11)	0.143(8)	2.42(4)						
6	1.339(9)	0.142 (9)	2.41(4)	1.338(12)	0.141(9)	2.40(4)						

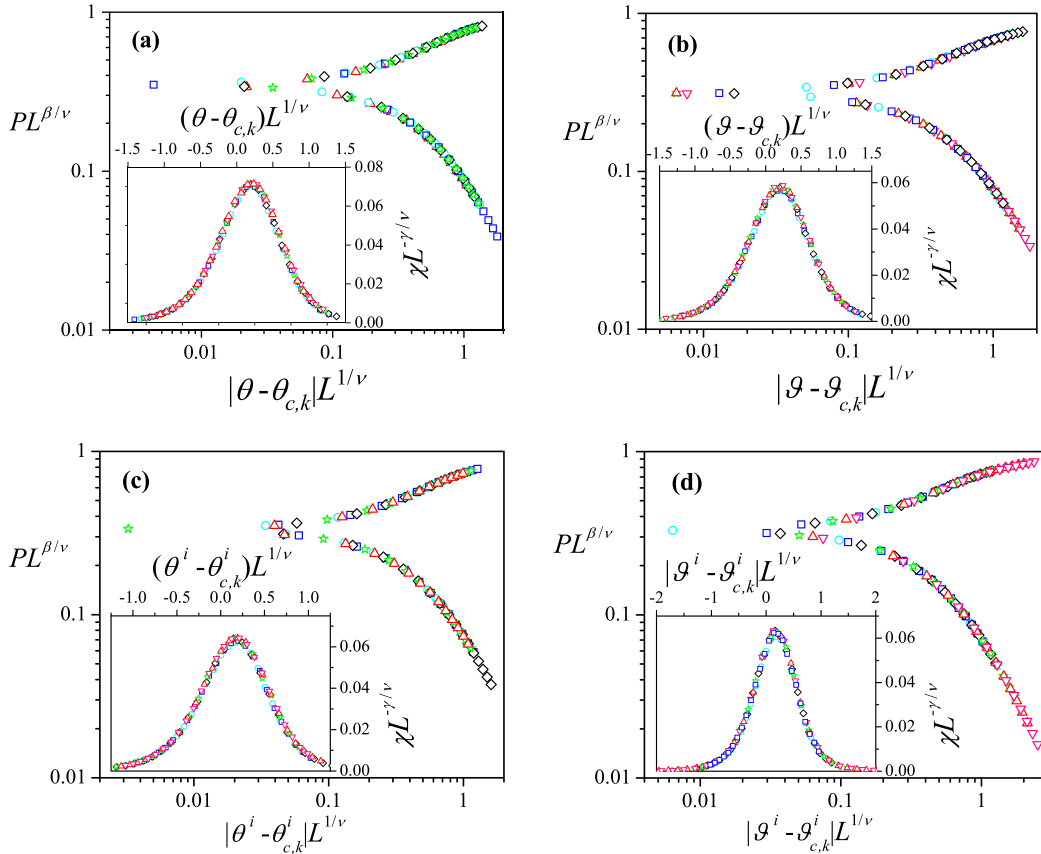


FIG. 18. Data collapsing of the percolation order parameter, $PL^{\beta/\nu}$ vs $|x - x_{c,k}|L^{1/\nu}$, and of the susceptibility, $\chi L^{-\gamma/\nu}$ vs $(x - x_{c,k})L^{1/\nu}$ (inset), for $k = 2$ and four different cases: (a) standard percolation and isotropic deposition model ($x = \theta$); (b) standard percolation and nematic deposition model ($x = \vartheta$); (c) inverse percolation and isotropic removal model ($x = \theta^i$); and (d) inverse percolation and nematic removal model ($x = \vartheta^i$). The plots were made using $\theta_{c,k=2} = 0.52487(3)$, $\vartheta_{c,k=2} = 0.49854(2)$, $\theta_{c,k=2}^i = 0.47513(3)$, $\vartheta_{c,k=2}^i = 0.50147(3)$ and the exact percolation exponents $\nu = 4/3$, $\beta = 5/36$, and $\gamma = 43/18$. Different symbols correspond to different lattice sizes: circles, $L = 128$; squares, $L = 192$; diamonds, $L = 256$; stars, $L = 384$; up triangles, $L = 512$; and down triangles, $L = 640$.

properties of the systems presented here correspond to the same universality class as the random percolation problem. This is of course true for the small range of k values where percolation is achieved; for larger values of this parameter this analysis is not possible.

V. CONCLUSIONS

In this paper, standard and inverse percolation properties of triangular tiles of side k (k -tiles) on triangular lattices have been studied by numerical simulations and finite-size scaling analysis. Two models have been addressed: the isotropic model, where the deposition (removal) of the triangular objects occurs with the same probability in any lattice direction; and the perfectly oriented model, where one lattice direction is privileged for depositing (removing) the k -tiles. In both cases (deposition and removal), the desired lattice coverage is reached following a generalized random sequential adsorption (RSA) mechanism.

First, the dependence of the jamming coverage $\theta_{j,k}$ on the size k was studied for standard deposition, the isotropic model, and k ranging from 2 to 32. The results are in excellent agreement with previous data in the literature [19,20,41]. By fitting the simulation data, it was found that

$\theta_{j,k} = 0.5540(4) + 0.530(3)/k - 0.084(2)/k^2$. According to this equation, the jamming coverage $\theta_{j,k}$ rapidly decreases for small values of k and asymptotically converges towards a definite value for infinitely large k -tiles $\theta_{j,k=\infty} = 0.5540(4)$. This value is less than the value $\theta_{j,k=\infty} = 0.5976(5)$ obtained for linear k -mers on triangular lattices [23], showing that linear k -mers are more effective in filling the lattice than k -tiles.

It was demonstrated that the removal process of k -tiles from the original lattice is equivalent to a RSA process of k -tiles on the complementary lattice. Each empty (occupied) site of the original lattice transforms into a occupied (empty) one of the complementary lattice. On the basis of these arguments, it is straightforward to conclude that $\theta_{j,k}^i = 1 - \theta_{j,k}$, where $\theta_{j,k}^i$ represents the inverse jamming coverage corresponding to the removal process. In the present case, $\theta_{j,k}^i$ can be written as $\theta_{j,k}^i = 0.4460 - 0.530/k + 0.084/k^2$ ($k \geq 2$).

Once the limiting parameters $\theta_{j,k}$ and $\theta_{j,k}^i$ were determined, the percolation properties of the isotropic system were studied. It was found that the standard (inverse) percolation threshold $\theta_{c,k}$ ($\theta_{j,k}^i$) increases (decreases) monotonically with increasing k up to $k = 6$. For $k \geq 7$, all jammed configurations are nonpercolating (percolating) states, and, consequently, the percolation phase transition disappears. This implies that for

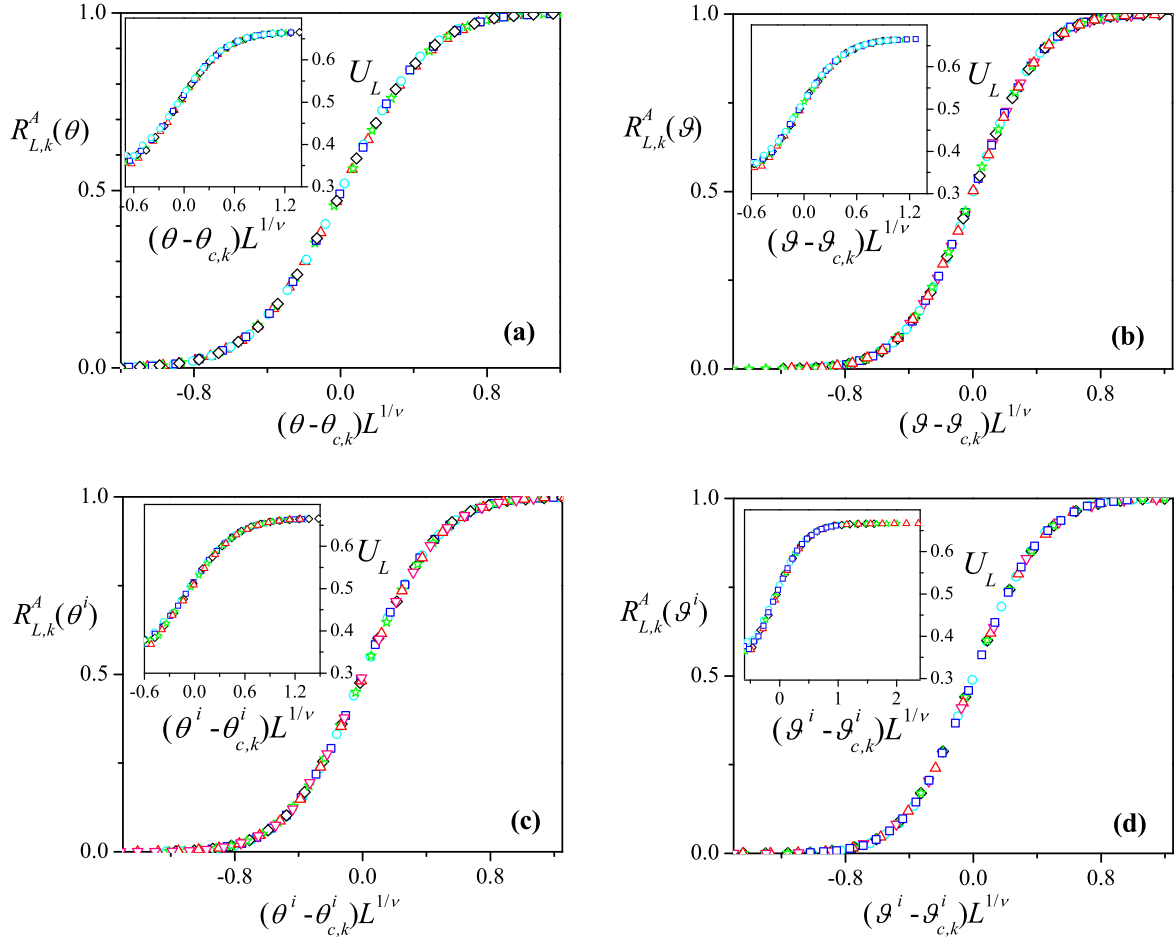


FIG. 19. Data collapsing of the percolation probability, $R_{L,k}^A(x)$ vs $(x - x_{c,k})L^{1/\nu}$, and the cumulant, U_L vs $(x - x_{c,k})L^{1/\nu}$ (inset), for $k = 2$ and four different cases: (a) standard percolation and isotropic deposition model ($x = \theta$); (b) standard percolation and nematic deposition model ($x = \vartheta$); (c) inverse percolation and isotropic removal model ($x = \theta^i$); and (d) inverse percolation and nematic removal model ($x = \vartheta^i$). The plots were made using $\theta_{c,k=2} = 0.52487(3)$, $\vartheta_{c,k=2} = 0.49854(2)$, $\theta_{c,k=2}^i = 0.47513(3)$, $\vartheta_{c,k=2}^i = 0.50147(3)$ and the exact percolation exponent $\nu = 4/3$. Different symbols correspond to different lattice sizes: circles, $L = 128$; squares, $L = 192$; diamonds, $L = 256$; stars, $L = 384$; up triangles, $L = 512$; and down triangles, $L = 640$.

larger values of k ($k > 6$) the jamming critical concentration occurs before the percolation phase transition.

The existence of a maximum value of k (in this case, $k_{\max} = 6$) from which the percolation phase transition no longer occurs reinforces the arguments given in Ref. [42]. Namely, when the dimension of the lattice is the same as the dimension of the depositing object, which is the case considered here, the percolation threshold is an increasing function of the size k in the range $[k \leq k_{\max}]$ and, for $k > k_{\max}$, the percolation phase transition disappears. This behavior has been observed in a wide variety of systems [1,5,33–35,42].

In addition, and as observed for linear k -mers on triangular lattices [26], a complementarity property between the percolation thresholds for standard and inverse percolation is found: $\theta_{c,k} + \theta_{c,k}^i = 1$. This complementarity property is a typical property of the triangular lattice [54,55].

Regarding the perfectly oriented case, the problem of aligned k -tiles deposited on triangular lattices was studied here for the first time. The jamming coverage dependence on the size k follows a decreasing law: $\vartheta_{j,k} = 0.36619(8) + 0.5565(8)/k + 0.5565(8)/k^2$, being $A =$

$\vartheta_{j,k=\infty} = 0.36619(8)$ less than the value $\theta_{j,k=\infty} = 0.5540(4)$ obtained for the isotropic case. These results are qualitatively different from those obtained for straight rigid k -mers, where the limit jamming for isotropic straight rigid k -mers is less than the limit jamming for aligned straight rigid k -mers [23,44,60]. In addition, the jamming coverage for the inverse problem $\vartheta_{j,k}^i$ can be written as $\vartheta_{j,k}^i = 1 - \vartheta_{j,k} = 0.63381 - 0.5565/k - 0.199/k^2$ ($k \geq 2$).

It was also found that, for the nematic deposition and removal problem, the percolation phase transition occurs only for $k = 2$, $k = 3$, and $k = 4$. For $k \geq 5$, the percolation phase transition disappears. In addition, and as in the isotropic case, the sum of standard and inverse percolation thresholds equals one ($\vartheta_{c,k} + \vartheta_{c,k}^i = 1$, $k = 2, 3, 4$), confirming the generality of this behavior in triangular lattices. Thus, the simple complementarity relationship between standard and inverse percolation thresholds seems to be a property typical for the triangular lattice, regardless of isotropic or oriented deposition or removal.

The isotropic and nematic inverse percolation problems were analyzed in terms of robustness. The obtained results

indicate that the percolating area for the isotropic case is larger than the corresponding percolating area for the nematic case. This means that the phase of occupied sites is more robust when the k -tiles are removed isotropically. Or, in other words, it is easier to disconnect the system when the k -tiles are removed according the nematic scheme. A contrary behavior has been observed for inverse percolation of straight rigid k -mers on triangular lattices [26], where the system is more robust when the removed needles are aligned in only one direction.

The complete set of percolation critical exponents ν , β , and γ was determined. The results obtained confirm that the percolation phase transition involved in the system, which occurs for k varying between 1 and 5(3) for the isotropic (nematic) problem, belongs to the same universality class as the standard two-dimensional percolation. Even though the geometry of the percolating object drastically affects the behavior of the percolation threshold as a function of the k size, it does not alter the nature of the percolation transition occurring in the system. In addition, the critical exponent characterizing the

jamming process (ν_j) was measured for isotropic and nematic schemes and for different values of k ranging between $k = 2$ and $k = 32$. In all cases, the values obtained for ν_j remain close to one, confirming that $\nu_j = 2/d$ for RSA processes on d -dimensional Euclidean lattices [61].

Future efforts will be devoted to extending the present analysis to bilayer and n -layer systems (with $n > 2$).

ACKNOWLEDGMENTS

This work was supported in part by CONICET (Argentina) under Project No. PIP 112-201101-00615; Universidad Nacional de San Luis (Argentina) under Project No. 03-1920; Ministry of Higher Education, Science and Technology, MESCYT-Dominican Republic, under Project FONDOCYT-2020-2021-1A2-112. The numerical work was done using the BACO parallel cluster located at Instituto de Física Aplicada, Universidad Nacional de San Luis - CONICET, San Luis, Argentina. One of the authors (NMDLCF) thanks the Idelisa Bonnelly Women in Science Scholarship Program, Youth Ministry, Dominican Republic.

-
- [1] D. Stauffer and A. Aharony, *Introduction to Percolation Theory* (Taylor & Francis, London, 2003).
 - [2] M. Sahimi, *Applications of Percolation Theory* (Taylor & Francis, London, 1992).
 - [3] G. Grimmett, *Percolation* (Springer-Verlag, Berlin, 1999).
 - [4] B. Bollobás and O. Riordan, *Percolation* (Cambridge University Press, New York, 2006).
 - [5] J. W. Evans, *Rev. Mod. Phys.* **65**, 1281 (1993).
 - [6] P. L. Krapivsky, S. Redner, and E. Ben-Naim, *A Kinetic View of Statistical Physics* (Cambridge University Press, Cambridge, 2010).
 - [7] S. N. Dorogovtsev and J. F. F. Mendes, *Evolution of Networks: From Biological Nets to the Internet and WWW* (Oxford University Press, Oxford, 2003).
 - [8] M. E. J. Newman, A.-L. Barabási, and D. J. Watts, *The Structure and Dynamics of Networks* (Princeton University Press, New Jersey, 2006).
 - [9] M. E. J. Newman, *Networks: An Introduction* (Oxford University Press, Oxford, 2010).
 - [10] R. Cohen and S. Havlin, *Complex Networks, Structure, Robustness and Function* (Cambridge University Press, Cambridge, 2010).
 - [11] Y. Kornbluth, S. Lowinger, G. A. Cwilich, and S. V. Buldyrev, *Phys. Rev. E* **89**, 032808 (2014).
 - [12] S. Lowinger, G. A. Cwilich, and S. V. Buldyrev, *Phys. Rev. E* **94**, 052306 (2016).
 - [13] Z. Gao and Z. R. Yang, *Physica A (Amsterdam, Neth.)* **255**, 242 (1998).
 - [14] A. Coniglio, *J. Phys.: Condens. Matter* **13**, 9039 (2001).
 - [15] E. Kenah and J. M. Robins, *Phys. Rev. E* **76**, 036113 (2007).
 - [16] A. Yazdi, H. Hamzeshpour, and M. Sahimi, *Phys. Rev. E* **84**, 046317 (2011).
 - [17] A. P. Chatterjee, *J. Chem. Phys.* **140**, 204911 (2014).
 - [18] Y. Y. Tarasevich, N. I. Lebovka, I. V. Vodolazskaya, A. V. Eserkepov, V. A. Goltseva, and V. V. Chirkova, *Phys. Rev. E* **98**, 012105 (2018).
 - [19] L. Budinski-Petković and U. Kozmidis-Luburić, *Phys. Rev. E* **56**, 6904 (1997).
 - [20] L. Budinski-Petković, I. Lončarević, M. Petković, Z. M. Jakšić, and S. B. Vrhovac, *Phys. Rev. E* **85**, 061117 (2012).
 - [21] L. Budinski-Petković, I. Lončarević, Z. M. Jakšić, S. B. Vrhovac, and N. M. Švrakić, *Phys. Rev. E* **84**, 051601 (2011).
 - [22] L. Budinski-Petković, I. Lončarević, Z. M. Jakšić, and S. B. Vrhovac, *J. Stat. Mech.* (2016) 053101.
 - [23] E. J. Perino, D. A. Matoz-Fernandez, P. M. Pasinetti, and A. J. Ramirez-Pastor, *J. Stat. Mech.* (2015) P10011.
 - [24] L. S. Ramirez, P. M. Centres, and A. J. Ramirez-Pastor, *J. Stat. Mech.* (2017) 113204.
 - [25] P. Longone, P. M. Centres, and A. J. Ramirez-Pastor, *Phys. Rev. E* **100**, 052104 (2019).
 - [26] L. S. Ramirez, P. M. Pasinetti, W. Lebrecht, and A. J. Ramirez-Pastor, *Phys. Rev. E* **104**, 014101 (2021).
 - [27] Y. Leroyer and E. Pommiers, *Phys. Rev. B* **50**, 2795 (1994).
 - [28] G. Kondrat and A. Pękaliski, *Phys. Rev. E* **63**, 051108 (2001).
 - [29] Y. Y. Tarasevich, N. I. Lebovka, and V. V. Laptev, *Phys. Rev. E* **86**, 061116 (2012).
 - [30] M. G. Slutskii, L. Y. Barash, and Y. Y. Tarasevich, *Phys. Rev. E* **98**, 062130 (2018).
 - [31] P. Longone, P. M. Centres, and A. J. Ramirez-Pastor, *Phys. Rev. E* **85**, 011108 (2012).
 - [32] T. Schilling, M. A. Miller, and P. van der Schoot, *Europhys. Lett.* **111**, 56004 (2015).
 - [33] M. Nakamura, *J. Phys. A: Math. Gen.* **19**, 2345 (1986).
 - [34] M. Nakamura, *Phys. Rev. A* **36**, 2384 (1987).
 - [35] A. J. Ramirez-Pastor, P. M. Centres, E. E. Vogel, and J. F. Valdés, *Phys. Rev. E* **99**, 042131 (2019).
 - [36] J. Feder, *J. Theor. Biol.* **87**, 237 (1980).
 - [37] B. J. Brosilow, R. M. Ziff, and R. D. Vigil, *Phys. Rev. A* **43**, 631 (1991).
 - [38] V. Privman, J.-S. Wang, and P. Nielaba, *Phys. Rev. B* **43**, 3366 (1991).
 - [39] G. J. Rodgers, *Phys. Rev. E* **48**, 4271 (1993).

- [40] L. S. Ramirez, P. M. Centres, and A. J. Ramirez-Pastor, *Phys. Rev. E* **100**, 032105 (2019).
- [41] D. Dujak, A. Karač, L. Budinski-Petković, Z. M. Jakšić, and S. B. Vrhovac, *Eur. Phys. J. B* **95**, 143 (2022).
- [42] A. C. Buchini Labayen, P. M. Centres, P. M. Pasinetti, and A. J. Ramirez-Pastor, *Phys. Rev. E* **100**, 022136 (2019).
- [43] G. D. García, F. O. Sanchez-Varretti, P. M. Centres, and A. J. Ramirez-Pastor, *Physica A (Amsterdam, Neth.)* **436**, 558 (2015).
- [44] B. Bonnier, M. Hontebeyrie, Y. Leroyer, C. Meyers, and E. Pommiers, *Phys. Rev. E* **49**, 305 (1994).
- [45] J. Hoshen and R. Kopelman, *Phys. Rev. B* **14**, 3438 (1976).
- [46] F. Yonezawa, S. Sakamoto, and M. Hori, *Phys. Rev. B* **40**, 636 (1989).
- [47] S. Biswas, A. Kundu, and A. K. Chandra, *Phys. Rev. E* **83**, 021109 (2011).
- [48] A. K. Chandra, *Phys. Rev. E* **85**, 021149 (2012).
- [49] K. Binder, *Rep. Prog. Phys.* **60**, 487 (1997).
- [50] J. Cardy, *J. Phys. A: Math. Gen.* **25**, L201 (1992).
- [51] J. J. H. Simmons, P. Kleban, and R. M. Ziff, *J. Phys. A: Math. Theor.* **40**, F771 (2007).
- [52] G. M. T. Watts, *J. Phys. A: Math. Gen.* **29**, L363 (1996).
- [53] N. Vandewalle, S. Galam, and M. Kramer, *Eur. Phys. J. B* **14**, 407 (2000).
- [54] R. M. Ziff and C. R. Scullard, *J. Phys. A: Math. Gen.* **39**, 15083 (2006).
- [55] R. M. Ziff, *Phys. Rev. E* **73**, 016134 (2006).
- [56] L. S. Ramirez, P. M. Centres, and A. J. Ramirez-Pastor, *J. Stat. Mech.* (2015) P09003.
- [57] L. S. Ramirez, P. M. Centres, A. J. Ramirez-Pastor, and W. Lebrecht, *J. Stat. Mech.* (2019) 113205.
- [58] G. A. Iglesias Panuska, P. M. Centres, and A. J. Ramirez-Pastor, *Phys. Rev. E* **102**, 032123 (2020).
- [59] S. S. Akimenko, A. V. Myshlyavtsev, M. D. Myshlyavtseva, V. A. Gorbunov, S. O. Podgornyi, and O. S. Solovyeva, *Phys. Rev. E* **105**, 044104 (2022).
- [60] A. Rényi, *Sel. Transl. Math. Stat. Probab.* **4**, 203 (1963); *Magyar Tud. Akad. Mat. Kutató Int. Közl.* **3**, 109 (1958).
- [61] P. M. Pasinetti, L. S. Ramirez, P. M. Centres, A. J. Ramirez-Pastor, and G. A. Cwilich, *Phys. Rev. E* **100**, 052114 (2019).